

Quantum random walk and tight-binding model subject to projective measurements at random times

Debraj Das

Department of Engineering Mathematics, University of Bristol, Bristol BS8 1TW,
United Kingdom

E-mail: debraj.das@bristol.ac.uk

Shamik Gupta

Department of Physics, Ramakrishna Mission Vivekananda Educational and
Research Institute, Belur Math, Howrah 711202, India

E-mail: shamikg1@gmail.com

Abstract. What happens when a quantum system undergoing unitary evolution in time is subject to repeated projective measurements to the initial state at random times? A question of general interest is: How does the survival probability S_m , namely, the probability that an initial state survives even after m number of measurements, behave as a function of m ? We address these issues in the context of two paradigmatic quantum systems, one, the quantum random walk evolving in discrete time, and the other, the tight-binding model evolving in continuous time, with both defined on a one-dimensional periodic lattice with a finite number of sites N . For these two models, we present several numerical and analytical results that hint at the curious nature of quantum measurement dynamics. In particular, we unveil that when evolution after every projective measurement continues with the projected component of the instantaneous state, the average and the typical survival probability decay as an exponential in m for large m . By contrast, if the evolution continues with the leftover component, namely, what remains of the instantaneous state after a measurement has been performed, the survival probability exhibits two characteristic m values, namely, $m_1^*(N) \sim N$ and $m_2^*(N) \sim N^\delta$ with $\delta > 1$. These scales are such that (i) for m large and satisfying $m < m_1^*(N)$, the decay of the survival probability is as m^{-2} , (ii) for m satisfying $m_1^*(N) \ll m < m_2^*(N)$, the decay is as $m^{-3/2}$, while (iii) for $m \gg m_2^*(N)$, the decay is as an exponential. The results for the dynamics with the leftover component, already known for the case of measurements at regular intervals, are being extended here to the case of measurements at random intervals. We find that our results hold independently of the choice of the distribution of times between successive measurements, as have been corroborated by our results for a wide range of distributions including exponential and power-law distributions as well as for the case of measurements at regular intervals. This fact hints at robustness and ubiquity of our derived results.

1. Introduction

Consider a quantum system described by a time-independent Hamiltonian H . Its state at any time t is characterized by a state vector $|\psi(t)\rangle$ defined in the Hilbert space \mathcal{H}_S of the system (S). The state vector undergoes unitary evolution in time as $|\psi(t)\rangle = U(t, t_0) |\psi(t_0)\rangle$; $t > t_0$, where $U(t, t_0) \equiv \exp(-iH(t - t_0))$ is the time-evolution operator [1]. Consider next a series of instantaneous measurements performed on the system at random times. Following the measurement postulate of quantum mechanics [2], each measurement involves projecting the instantaneous state of the system onto the Hilbert space $\mathcal{H}_D \subset \mathcal{H}_S$ of the measuring device (D). Starting at time $t = 0$ with a state vector with unit norm, it is evident that each projective measurement reduces the norm, and we may ask for its magnitude after a certain number $m \in \mathbb{Z}^+$ of measurements have been performed on the system. The norm of the state vector at any time $t > 0$ has the physical interpretation of survival probability of the initial state at that time instant. To see this, consider a quantum particle undergoing motion in a spatial domain \mathcal{D} . It then follows that $|\psi(\mathbf{r}, t)|^2 d^3\mathbf{r}$ gives the probability of finding the particle between locations \mathbf{r} and $\mathbf{r} + d\mathbf{r}$ in \mathcal{D} at time t , with $\psi(\mathbf{r}, t) \equiv \langle \mathbf{r} | \psi(t) \rangle$. With $\int_{\mathcal{D}} d^3\mathbf{r} |\psi(\mathbf{r}, t = 0)|^2 = 1$ so that the particle is initially for sure within \mathcal{D} , and with m instantaneous projective measurements performed on the system at random times $t_1, t_2, t_3, \dots, t_m$, with $0 < t_1 < t_2 < t_3 < \dots < t_m$, the norm of the state vector at time t_m given by $\langle \psi(t_m) | \psi(t_m) \rangle = \int_{\mathcal{D}} d^3\mathbf{r} |\psi(\mathbf{r}, t_m)|^2$ gives the probability S_m that the particle is still inside \mathcal{D} at the end of m projective measurements. In other words, S_m is the survival probability that the particle has survived in \mathcal{D} up to time t_m . With the definition $t_0 = 0$, note that $S_0 = 1$. For latter purpose, let us define the quantity

$$F_m \equiv S_{m-1} - S_m, \quad (1)$$

which stands for the first-detection probability, namely, the probability that the particle gets detected by the measuring device at time t_m *for the first time*. It is pertinent to ask: How does S_m vary from one realization of random times $\{t_1, t_2, \dots, t_m\}$ to another? What is the dependence on m of $\overline{S_m}$, the averaged survival probability? How does the typical value of the survival probability, as measured in a typical realization of the random times, depend on m ?

In the aforementioned protocol, we may consider the successive time gaps $\tau_\alpha \equiv t_\alpha - t_{\alpha-1}$; $\alpha = 1, 2, 3, \dots, m$ to be random variables sampled independently from a common distribution $p(\tau)$, that is to say, the τ_α 's are independent and identically-distributed (i.i.d.) random variables. In this backdrop, let us be more specific with the framework of our study. Consider a generic state $|\psi(0)\rangle$ evolving for a random time τ_1 according to the unitary operator $U_1 \equiv \exp(-iH\tau_1)$. The evolved state $U_1|\psi(0)\rangle$ is then subject to an instantaneous projective measurement according to a given projection operator P . Subsequent evolution may then proceed with either the projected component $PU_1|\psi(0)\rangle$ of the state $U_1|\psi(0)\rangle$ or its leftover component given by $(\mathbb{I} - P)U_1|\psi(0)\rangle$, where \mathbb{I} is the identity operator. We then iterate m times the

aforementioned set of events, so we have two different schemes of time evolution of the system involving one of the following repetitive sequence of event-pair:

- Scheme 1:** A unitary evolution for a random time τ_α according to the unitary operator $U_\alpha \equiv \exp(-iH\tau_\alpha)$, followed by the action of the operator P . This scheme corresponds to subsequent evolution with the projected component after each measurement.
- Scheme 2:** A unitary evolution for a random time τ_α according to the unitary operator U_α , followed by the action of the operator $\tilde{P} \equiv \mathbb{I} - P$. This scheme corresponds to subsequent evolution with the leftover component after each measurement.

A typical time evolution for a given realization $\{\tau_\alpha\}_{1 \leq \alpha \leq m}$ is shown in Fig. 1. We will take the projection operator to be performing projection to the initial state:

$$P = |\psi(0)\rangle\langle\psi(0)|. \quad (2)$$

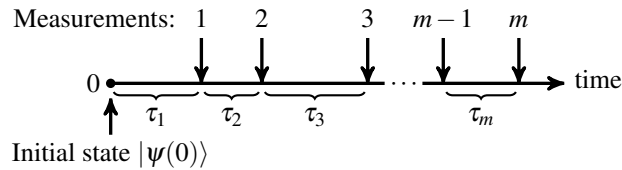


Figure 1. A typical time evolution of a quantum system subject to projective measurements at random times, as detailed in the text. Starting from the state $|\psi(0)\rangle$, the evolution involves the following repetitive sequence of events: unitary evolution for time according to operator U_α for time τ_α followed by a projective measurement (denoted by the down arrows). In **Scheme 1** (respectively, **Scheme 2**), subsequent evolution at the end of each measurement is carried out with the projected component of the instantaneous state (respectively, the leftover component).

In the following, we will use the notation $|\psi_\alpha^{(b)}\rangle$ (respectively, $|\psi_\alpha^{(a)}\rangle$) to denote the state of the system at the end of evolution for time τ_α and just before (respectively, just after) the α -th projective measurement. It is evident from the dynamical rules of evolution that $|\psi_\alpha^{(b)}\rangle = U_\alpha |\psi_{\alpha-1}^{(a)}\rangle$, while $|\psi_\alpha^{(a)}\rangle$ will be either $|\psi_\alpha^{(a)}\rangle = P |\psi_\alpha^{(b)}\rangle$ (**Scheme 1**) or $|\psi_\alpha^{(a)}\rangle = \tilde{P} |\psi_\alpha^{(b)}\rangle$ (**Scheme 2**), and $\alpha = 1, 2, \dots, m$. We define the random variable

$$S_m \equiv S_m(\{\tau_\alpha\}_{1 \leq \alpha \leq m}) = \langle \psi_m^{(a)} | \psi_m^{(a)} \rangle \quad (3)$$

as the survival probability of the initial state after m projective measurements and for the realization $\{\tau_\alpha\}_{1 \leq \alpha \leq m}$. Note that different values of S_m correspond to different total duration of evolution $\mathcal{T} \equiv \sum_{\alpha=1}^m \tau_\alpha$. We may then ask: How does \bar{S}_m depend on m ? How does the dependence vary between **Scheme 1** and **Scheme 2**? What is the essential role played by $p(\tau)$ in dictating the value of \bar{S}_m in the two schemes?

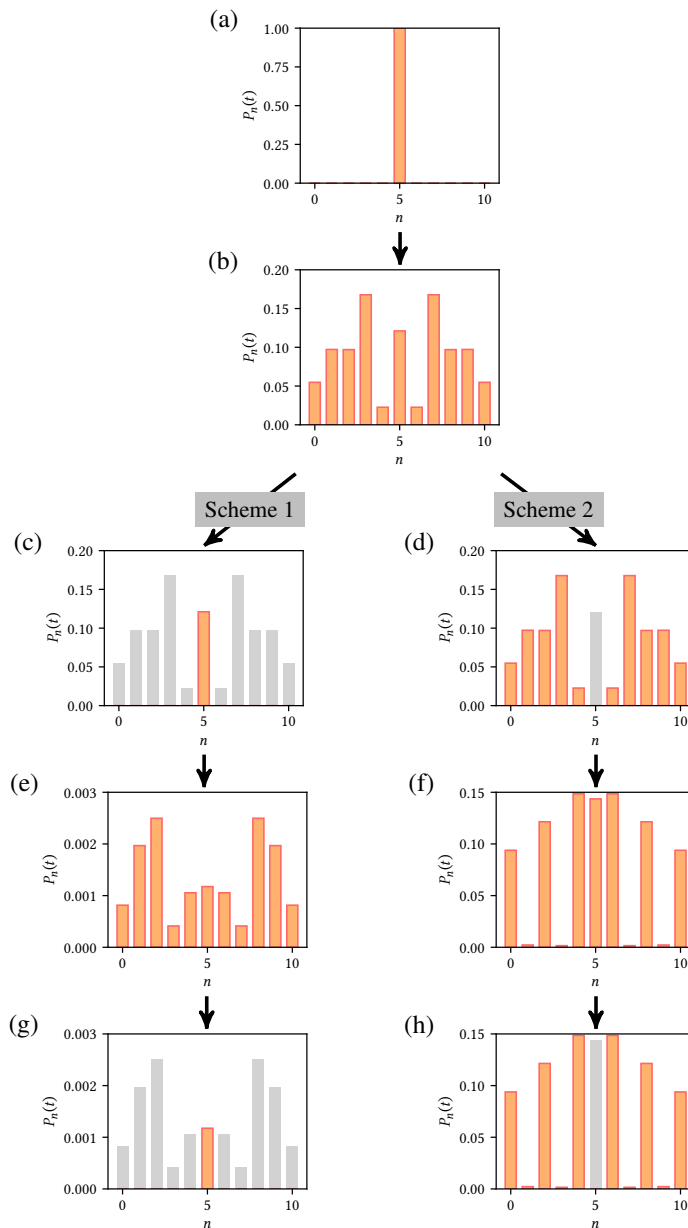


Figure 2. Schematic representation of the dynamics studied in the paper under **Scheme 1** and **Scheme 2**. For a quantum particle moving between the sites of a one-dimensional lattice, the different panels show the site-occupation probability at different times: panel (a) corresponds to the initial instant $t = 0$, panel (b) corresponds to the situation just before the first projective measurement is performed on the system at time $t = t_1$. Panels (c) and (d) denote $P_n(t)$ corresponding respectively to the projected and the leftover state just following the first measurement. In **Scheme 1** (respectively, **Scheme 2**), subsequent evolution following each projective measurement is carried out with the projected state (respectively, the leftover state). Correspondingly, panels (e) and (f) represent the state just before the second projective measurement performed at time t_2 and is the result of unitary evolution of the state represented by panels (c) and (d), respectively. Finally, panels (g) and (h) represent respectively the projected and the leftover state corresponding to panels (e) and (f), respectively. The grey bars in these panels show the part of the site-occupation probability that has been projected out by the process of measurement.

To illustrate with an example the two schemes of dynamical evolution, consider the representative example of a quantum particle moving between the sites of a one-dimensional lattice. Referring to Fig. 2, wherein n labels the lattice sites, the particle starts its journey at time $t = 0$ from site $n = 5$ in a lattice of 11 sites [3]. With the ket vector $|n\rangle$ denoting the state of the particle on site n and satisfying $\langle n|m\rangle = \delta_{nm}$ and $\sum_n |n\rangle\langle n| = \mathbb{I}$, the initial state vector is $|\psi(0)\rangle = |5\rangle$. In Fig. 2, the different panels show the site occupation probability $P_n(t) = |\langle n|\psi(t)\rangle|^2$, where $|\psi(t)\rangle$ is the state vector at time t . Panel (a) depicts $P_n(t = 0) = \delta_{n,5}$. The first projective measurement is performed on the system at time $t_1 > 0$. Panel (b) shows $P_n(t)$ just before the first measurement and is the result of unitary evolution of the state in panel (a), while panels (c) and (d) show respectively results corresponding to the projected and the leftover state just after the first measurement, the state being denoted by the generic symbol $|\psi_1^{(a)}\rangle$. The grey bars in these panels show the part of $P_n(t_1)$ that has been projected out by the process of measurement. In **Scheme 1** (respectively, **Scheme 2**), subsequent unitary evolution proceeds with the state corresponding to panel (c) (respectively, panel (d)). If the second measurement happens at time $t_2 > t_1$, the state $|\psi_2^{(b)}\rangle$ corresponds to panels (e) and (f) in the two schemes and is the outcome of unitary evolution of panels (c) and (d), respectively. Panels (g) and (h) show the results for the state $|\psi_2^{(a)}\rangle$ just after the second measurement and represent similar to panels (c) and (d) the projected and the leftover state, respectively. One goes on repeating the above sequence of event-pair: unitary evolution, subsequent evolution with either the projected state (**Scheme 1**) or the leftover state (**Scheme 2**). In terms of $|\psi_m^{(a)}\rangle$, the site occupation probability just after the m -th measurement reads

$$P_n(t = t_m^{(a)}) = |\langle n|\psi_m^{(a)}\rangle|^2, \quad (4)$$

with $t_m^{(a)}$ denoting the time instant just after the m -th measurement. On the other hand, the survival probability in the two schemes is related to the respective $P_n(t)$ as

$$S_m = \sum_n P_n(t = t_m^{(a)}). \quad (5)$$

Thus, the survival probability is nothing but a measure of the site-averaged occupation probability of the particle in the two schemes.

The so-called quantum Zeno effect, first discussed in a seminal paper by Sudarshan and Misra in 1977 [4], is a curious quantum mechanical phenomenon involving a quantum system subject to projective measurements to a given initial state at regular time intervals (stroboscopic measurements). In the extreme case of a frequent-enough series of measurements over a fixed total duration (implying thereby that the successive measurements are infinitesimally close to one another), the survival probability for the system to remain in the initial state may be shown to approach unity in the limit of an infinite number of measurements, i.e., the dynamical evolution of the system gets completely frozen in time. Subsequently, stochastic quantum Zeno effect was introduced to study the situation in which the measurements are randomly spaced in time [5]. It

is important to remark in the context of the present work that the Zeno effect involves evolution following each measurement to be carried out with the projected component of the instantaneous state, while it is evidently of interest to investigate the dynamics in the complimentary case in which it is the leftover component of the instantaneous state that undergoes evolution subsequent to each measurement. These two dynamical scenarios correspond respectively to **Scheme 1** dynamics and **Scheme 2** dynamics defined above. Performing measurements at random times is not quite an issue of only theoretical curiosity, but may be motivated on the ground that after all, any experiment that aims to employ projective measurements to demonstrate the Zeno effect would typically use a timer to time the gap between successive measurements. Because the timer would invariably be of finite precision, it would not be possible to ensure that measurements are performed at exactly regular time intervals. On the other hand, in the context of this paper, it is relatively easy to control the number of times that the projective measurement is repeated, thus justifying our dynamical set-ups. The average time between two intervals (averaged over different realizations of the intervals) would of course be finite in experiments.

In this work, we consider two representative quantum systems defined on a one-dimensional periodic lattice with a finite number of sites N , (i) the quantum random walk (QRW) model evolving in discrete times [6], and (ii) the tight-binding model (TBM), evolving in continuous time [7, 8]. Within the ambit of these two systems, we unveil a plethora of interesting results, numerical as well as analytical, including universal features in the late-time behavior of both the average and the typical survival probability, all of which point to the intriguing nature of quantum measurement process. We note that experimentally, it has been possible to implement a random or a stochastic sequence of measurement protocol [5, 9, 10, 11, 12], and hence we believe that our results are amenable to experimental realization.

The paper is organized as follows. We choose to study first the QRW, which is described in detail in Section 2.1. Here, we compute analytically the site occupation probability, the results of which form a crucial input for the analytical and semi-analytical description of the survival probability pursued in Section 2.2. This latter section contains our main results on the survival probability of a generic initial state subject to instantaneous projective measurements to the initial state at random times. We report extensive numerical results demonstrating that the average as well as the typical survival probability decays asymptotically as an exponential in m when the evolution following each projective measurement is carried on with the projected component of the instantaneous state. On the contrary, when the evolution proceeds with the leftover component, the survival probability exhibits two characteristic m values, namely, $m_1^*(N) \sim N$ and $m_2^*(N) \sim N^\delta$ with $\delta > 1$. We show that (i) for m large and satisfying $m < m_1^*(N)$, the decay of the survival probability is as m^{-2} (correspondingly, F_m decays as m^{-3}), (ii) for m satisfying $m_1^*(N) \ll m < m_2^*(N)$, the decay is as $m^{-3/2}$ (correspondingly, F_m decays as $m^{-5/2}$), while (iii) for $m \gg m_2^*(N)$, the decay is as an exponential. These results hold independently of the choice of the

distribution of times between successive measurements, as we demonstrate by our results for a wide range of distributions including exponential and power-law distributions as well as for the case of measurements at regular intervals. For the projected case, we support our numerical findings with explicit analytical calculations using large deviation theory (LDT) well known in probability theory [28, 29], while for the leftover case, a semi-analytical approach reproduces correctly our numerical findings.

Next, we turn to a description of the TBM and a discussion on its site occupation probability in Section 3.1. This is followed in Section 3.2 by a discussion of our numerical results for the survival probability for the case in which the evolution following each projective measurement is carried on with the projected component as well as for the case in which it is the leftover component of the instantaneous state that undergoes subsequent evolution until next measurement. Here too we support our findings with analytical results derived using the LDT for the projected case and with semi-analytic calculations for the leftover case. What form the heart of such calculations are our results on site occupation probability presented in Section 3.1. Similar to the case of the QRW, we find that for representative $p(\tau)$, the average as well as the typical survival probability decays as a function of m as an exponential for the projected case and is characterized by the two scales $m_1^*(N)$ and $m_2^*(N)$ with associated behaviours same as discussed above for the leftover case in the case of the QRW. Our results for the QRW and the TBM hint at the robustness of our results with respect to both discrete and continuous time evolution. The paper ends with conclusions in Section 4. The appendix collects some of the technical details of our analytical calculations.

The TBM and related systems when subject to projective measurements with time evolution following **Scheme 2** of dynamics have in recent years been studied to address the issue of when does a quantum particle evolving under the dynamics arrive at a chosen set of sites [13, 14, 15, 16, 17, 18, 19, 20, 21, 22, 23, 24, 25, 26, 27]. A crucial difference is that, barring [27], these contributions almost exclusively implement measurements at regular intervals of times, unlike the scheme considered in this work in which sequence of measurements at random times is implemented. While we will in later part of the paper discuss in some detail the contribution of this set of work, let us state right at the outset what new findings we report on with respect to these references. Both the quantum random walk and the tight-binding model have been extensively studied in the literature, and the question of first-detection probability has also been amply studied in the past. However, to the best of our knowledge, the issue of first-detection probability when measurements are done not at regular but at random time intervals and the ensuing results that we report in this work have not been reported so extensively in the literature. The fact that the survival probability S_m exhibits in appropriate regimes the decay as m^{-2} and as $m^{-3/2}$, that the first-detection probability F_m decays in appropriate regimes as m^{-3} and as $m^{-5/2}$ with oscillations at small m have all been known in the literature for the case of measurements at regular intervals (see, e.g., Refs. [13, 16]), and our main contribution as regards **Scheme 2** of the dynamics is to show that these results hold also when measurements are performed at random intervals, based on our

analysis for the studied distributions of these random intervals.

2. Quantum random walk (QRW) model

2.1. Model and site occupation probability

A quantum random walk (QRW) [6, 30, 31] is a quantum mechanical system evolving in discrete times, and involves a walker performing random walk on a lattice. We consider here the model on a one-dimensional periodic lattice of N sites. Let us label the sites by the index $n \in \mathbb{Z}$. The motion of the walker on the lattice depends on the state of a “quantum” coin that it carries. The Hilbert space \mathcal{H}_S of the walker system is given by a direct sum of the Hilbert space \mathcal{H}_P for the position of the walker on the lattice and spanned by the orthonormal basis states $\{|n\rangle\}$; $\langle m|n\rangle = \delta_{m,n}$, and of the Hilbert space \mathcal{H}_C for the coin and spanned by the orthonormal basis states $|\uparrow\rangle$ and $|\downarrow\rangle$ representing respectively the head state and the tail state of the coin. The walker state at any time t , denoted by $|\psi(t)\rangle$, is obtained as a linear combination of the basis states of the space \mathcal{H}_S with time-dependent expansion coefficients, where the basis states are given by a direct product of those of the position and the coin space. The coin space may also be thought of as a spin space of a spin-1/2 particle, with the basis states being the eigenstates, the up (u) and the down (d) state, of the z -component of the spin operator. The up and down states may then be taken to correspond respectively to the head and the tail state of the coin.

The random walker evolves according to the following repetitive sequence of events: acting on the walker state, first by a unitary operator $C \otimes \mathbb{I}$, and then by a unitary operator U , with both operations constituting one time step of evolution of the walker state. Here, U is given by

$$U \equiv |\uparrow\rangle\langle\uparrow| \otimes \sum_n |n+1\rangle\langle n| + |\downarrow\rangle\langle\downarrow| \otimes \sum_n |n-1\rangle\langle n|, \quad (6)$$

while C has the form

$$C \equiv \cos\theta |\uparrow\rangle\langle\uparrow| + \sin\theta |\uparrow\rangle\langle\downarrow| - \sin\theta |\downarrow\rangle\langle\uparrow| + \cos\theta |\downarrow\rangle\langle\downarrow|, \quad (7)$$

where $\theta \in [0, 2\pi)$ is a given parameter. The operator U generates a translation of the walker on the lattice that is conditioned on the state of the quantum coin, while the operator C generates a rotation in the coin space.

A large class of initial conditions corresponds to having the walker on a given site n_0 and in an arbitrary superposition of the coin states:

$$|\psi(0)\rangle = \frac{1}{\sqrt{|a|^2 + |b|^2}} (a|\uparrow\rangle + b|\downarrow\rangle) \otimes |n_0\rangle, \quad (8)$$

with $a, b \in \mathbb{C}$. Following the rules of evolution of the random walker detailed above, we

may write down explicitly the state of the walker at the first and the second time step:

$$\begin{aligned}
 |\psi(1)\rangle &= \frac{1}{\sqrt{|a|^2 + |b|^2}} \left([a \cos \theta |\uparrow\rangle + b \sin \theta |\uparrow\rangle] \otimes |n_0 + 1\rangle \right. \\
 &\quad \left. + [-a \sin \theta |\downarrow\rangle + b \cos \theta |\downarrow\rangle] \otimes |n_0 - 1\rangle \right), \\
 |\psi(2)\rangle &= \frac{1}{\sqrt{|a|^2 + |b|^2}} \left([a \cos^2 \theta |\uparrow\rangle + b \cos \theta \sin \theta |\uparrow\rangle] \otimes |n_0 + 2\rangle \right. \\
 &\quad + [-b \sin^2 \theta |\downarrow\rangle - a \cos \theta \sin \theta |\downarrow\rangle] \otimes |n_0\rangle \\
 &\quad + [-a \sin^2 \theta |\uparrow\rangle + b \cos \theta \sin \theta |\uparrow\rangle] \otimes |n_0\rangle \\
 &\quad \left. + [-a \cos \theta \sin \theta |\downarrow\rangle + b \cos^2 \theta |\downarrow\rangle] \otimes |n_0 - 2\rangle \right). \tag{9}
 \end{aligned}$$

It is evident then that the state at time t has the general structure

$$|\psi(t)\rangle = |\uparrow\rangle \otimes \sum_n \Psi_u(n, t) |n\rangle + |\downarrow\rangle \otimes \sum_n \Psi_d(n, t) |n\rangle, \tag{10}$$

where the sum extends over all the lattice sites. Here, $\Psi_u(n, t)$ and $\Psi_d(n, t)$ are respectively the probability amplitude to find the random walker on site n at time t with spin state up (u) and down (d). Normalization of $|\psi(t)\rangle$ implies $\sum_n P_n(t) = 1 \forall t$, with

$$P_n(t) \equiv |\Psi_u(n, t)|^2 + |\Psi_d(n, t)|^2 \tag{11}$$

being the site occupation probability for the random walker to be on site n at time t .

For $\theta = 0, \pi$, an inspection of Eq. (9) suggests that at any time step t , only the extreme possible sites to the left and to the right are going to be occupied. For $\theta = \pi/2, 3\pi/2$, Eq. (9) implies that the random walker is going to occupy sites $(n_0 \pm 1)$ at odd time steps and only the initial site n_0 at even time steps. These scenarios are a result of the operator C effectively implementing no mixing of the spin states $|\uparrow\rangle$ and $|\downarrow\rangle$ for $\theta = 0, \pi$, and a complete mixing implementing the transformations $|\uparrow\rangle \rightarrow -|\downarrow\rangle$ and $|\downarrow\rangle \rightarrow |\uparrow\rangle$ for $\theta = \pi/2$, and $|\uparrow\rangle \rightarrow |\downarrow\rangle$ and $|\downarrow\rangle \rightarrow -|\uparrow\rangle$ for $\theta = 3\pi/2$. Only for other values of θ , when there is partial mixing, do we get non-trivial results in which several sites are occupied at any time instant. In Table 1, we have listed possibilities for nonzero $P_n(t)$ for different choices of the initial location of the QRW and for N even and odd.

We now present analytical results on the site occupation probability $P_n(t)$ for the initial state (8). To proceed, we note that acting on the state (10) by C followed by U gives linear equations expressing $\Psi_{u,d}(n, t+1)$ in terms of $\Psi_{u,d}(n-1, t)$ and $\Psi_{u,d}(n+1, t)$, which may be put in the form of a matrix equation by introducing the two-component vector [30]

$$|\Psi(n, t)\rangle \equiv [\Psi_u(n, t) \quad \Psi_d(n, t)]^T. \tag{12}$$

N even		N odd			
Initial site n_0 even	Initial site n_0 odd	Initial site n_0 even		Initial site n_0 odd	
For all t	For all t	$t < N$	$t > N$	$t < N$	$t > N$
For even t : nonzero $P_n(t)$ only for even n .	For even t : nonzero $P_n(t)$ only for odd n .	For even t : nonzero $P_n(t)$ only for even n .	Non-zero $P_n(t)$ possible for all n and t .	For even t : nonzero $P_n(t)$ only for odd n .	Non-zero $P_n(t)$ possible for all n and t .
For odd t : nonzero $P_n(t)$ only for odd n .	For odd t : nonzero $P_n(t)$ only for even n .	For odd t : nonzero $P_n(t)$ only for odd n .		For odd t : nonzero $P_n(t)$ only for even n .	

Table 1. Site occupation probability $P_n(t)$ in the case of the QRW on a one-dimensional periodic lattice with N sites. Here, the initial state is given by Eq. (8).

Here, \top denotes transpose operation. Then, the matrix equation reads

$$|\Psi(n, t+1)\rangle = \begin{bmatrix} \cos \theta & \sin \theta \\ 0 & 0 \end{bmatrix} |\Psi(n-1, t)\rangle + \begin{bmatrix} 0 & 0 \\ -\sin \theta & \cos \theta \end{bmatrix} |\Psi(n+1, t)\rangle. \quad (13)$$

To solve Eq. (13), we employ the method of discrete Fourier transform [30], to write $|\tilde{\Psi}(k, t)\rangle = \sum_n |\Psi(n, t)\rangle \exp(i2\pi kn/N)$ and $|\Psi(n, t)\rangle = (1/N) \sum_k |\tilde{\Psi}(k, t)\rangle \exp(-i2\pi kn/N)$, with $n, k \in [-(N-1)/2, (N-1)/2]$ if N is odd, and $n, k \in [-N/2, N/2 - 1]$ if N is even. Equation (13) then gives

$$|\tilde{\Psi}(k, t)\rangle = (M_k)^t |\tilde{\Psi}(k, 0)\rangle, \quad (14)$$

where the matrix M_k is given by

$$M_k \equiv \begin{bmatrix} e^{i2\pi k/N} \cos \theta & e^{i2\pi k/N} \sin \theta \\ -e^{-i2\pi k/N} \sin \theta & e^{-i2\pi k/N} \cos \theta \end{bmatrix} = \lambda_k^{(1)} |\phi_k^{(1)}\rangle \langle \phi_k^{(1)}| + \lambda_k^{(2)} |\phi_k^{(2)}\rangle \langle \phi_k^{(2)}|, \quad (15)$$

in terms of its eigenvalues and orthonormal eigenvectors:

$$\begin{aligned} \lambda_k^{(1)} &= e^{i\omega_k}, & |\phi_k^{(1)}\rangle &= \frac{1}{\sqrt{1+h_+^2(k)}} \begin{bmatrix} -ie^{i2\pi k/N} h_+(k) \\ 1 \end{bmatrix}, \\ \lambda_k^{(2)} &= e^{-i\omega_k}, & |\phi_k^{(2)}\rangle &= \frac{1}{\sqrt{1+h_-^2(k)}} \begin{bmatrix} -ie^{i2\pi k/N} h_-(k) \\ 1 \end{bmatrix}, \end{aligned} \quad (16)$$

with $\cos \omega_k \equiv \cos(2\pi k/N) \cos \theta$, and $h_{\pm}(k) \equiv \cot \theta \sin(2\pi k/N) \pm \csc \theta \sin \omega_k$. Note that $h_+(-k) = -h_-(k)$, and $h_+(k)h_-(k) = -1$. The initial condition corresponding to Eq. (8) is $|\tilde{\Psi}(k, 0)\rangle = \left(\exp(i2\pi kn_0/N) / \sqrt{|a|^2 + |b|^2} \right) [a \ b]^\top \forall k$. Using these results to obtain $|\tilde{\Psi}(k, t)\rangle = (\lambda_k^{(1)})^t \langle \phi_k^{(1)} | \tilde{\Psi}(k, 0) \rangle |\phi_k^{(1)}\rangle + (\lambda_k^{(2)})^t \langle \phi_k^{(2)} | \tilde{\Psi}(k, 0) \rangle |\phi_k^{(2)}\rangle$, and then performing inverse Fourier transformation, we finally obtain for odd N the result

$$\Psi_u(n, t) = \sum_{k=-(N-1)/2}^{(N-1)/2} \mathcal{A}_u(k, n, t), \quad \Psi_d(n, t) = \sum_{k=-(N-1)/2}^{(N-1)/2} \mathcal{A}_d(k, n, t), \quad (17)$$

while for even N , we get

$$\begin{aligned}\Psi_{\text{u}}(n, t) &= (-1)^{n-n_0+t} \frac{\{a \cos(\theta t) + b \sin(\theta t)\}}{N \sqrt{|a|^2 + |b|^2}} + \sum_{k=-N/2+1}^{N/2-1} \mathcal{A}_{\text{u}}(k, n, t), \\ \Psi_{\text{d}}(n, t) &= (-1)^{n-n_0+t} \frac{\{-a \sin(\theta t) + b \cos(\theta t)\}}{N \sqrt{|a|^2 + |b|^2}} + \sum_{k=-N/2+1}^{N/2-1} \mathcal{A}_{\text{d}}(k, n, t).\end{aligned}\tag{18}$$

Here, the quantities $\mathcal{A}_{\text{u}}(k, n, t)$ and $\mathcal{A}_{\text{d}}(k, n, t)$ are given by

$$\begin{aligned}\mathcal{A}_{\text{u}}(k, n, t) &= \mathcal{N}(a, b, k) \left[a \cos\{2\pi k(n - n_0)/N + \omega_k t\} \right. \\ &\quad \left. + b h_+(k) \sin\{2\pi k(n - n_0 - 1)/N + \omega_k t\} \right], \\ \mathcal{A}_{\text{d}}(k, n, t) &= \mathcal{N}(a, b, k) \left[-a h_+(k) \sin\{-2\pi k(n - n_0 + 1)/N + \omega_k t\} \right. \\ &\quad \left. + b \cos\{-2\pi k(n - n_0)/N + \omega_k t\} \right],\end{aligned}\tag{19}$$

with $\mathcal{N}(a, b, k) = 2 / \left[N(1 + h_+^2(k)) \sqrt{|a|^2 + |b|^2} \right]$.

Let us remark that implementing the transformation $\theta \rightarrow \theta + \pi$ in the expression for C is tantamount to multiplying C and consequently the matrix M_k by the factor -1 . As a result, the eigenvalues of M_k get both multiplied by the factor -1 , although the corresponding eigenvectors remain the same. All of these would however leave $|\Psi_{\text{u}}(n, t)|^2$ and $|\Psi_{\text{d}}(n, t)|^2$ and consequently the site occupation probability $P_n(t)$ unchanged, thereby making us conclude that the QRW is invariant with respect to the transformation $\theta \rightarrow \theta + \pi$. Hence, we will in the rest of the paper restrict the values of θ to the range $[0, \pi]$.

In Fig. 3, we show a comparison between numerical results and theory for the site occupation probability $P_n(t)$, demonstrating a perfect match. In the figure, numerics correspond to bare evolution of the unitary dynamics of the model, while analytical results are given by Eqs. (11), (17) and (18).

2.2. Random projective measurements and survival probability

2.2.1. Numerical results

We now present numerical results on the survival probability S_m , and in particular, on the average and the typical survival probability, and their dependence on the number of measurements m . To proceed, we note in the context of the discussion on measurement schemes in Section 1 that the time intervals τ_α in the present case are positive integers with underlying discrete distribution p_τ [32]. Moreover, since the QRW evolves in discrete times, the unitary operator U_α is given by $U_\alpha \equiv [U(C \otimes \mathbb{I})]^\alpha$. Thus, a single-step evolution of the QRW involves acting by the operator $C \otimes \mathbb{I}$ followed by the operator U , see Eqs. (6) and (7). Since the QRW evolves in discrete times, the phrases ‘‘time’’ and ‘‘time step’’ would have the same meaning in the context of the QRW and would be used interchangeably in the following.

As a representative case for reporting our results, we take the QRW lattice size N to be even with $n_0 = 0$. It then follows from Table 1 that the site occupation

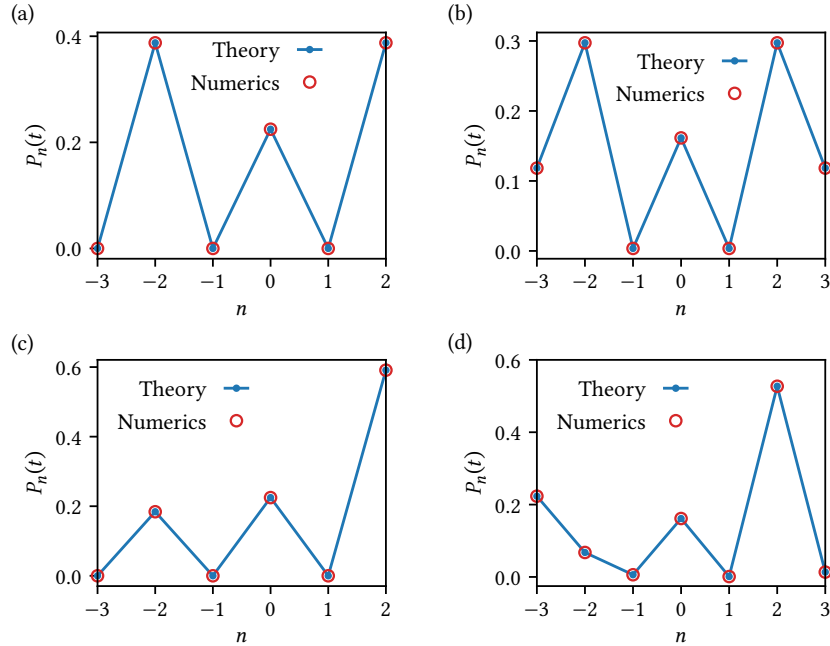


Figure 3. Site occupation probability $P_n(t)$ for the QRW on a one-dimensional periodic lattice of N sites and at time $t = 20$, while starting from the state (8) with $n_0 = 0$. The values of the parameters a and b defining the initial state are $a = 1$, $b = i$ for panels (a) and (b), and $a = b = 1$ for panels (c) and (d). The value of N is $N = 6$ for panels (a) and (c), and $N = 7$ for panels (b) and (d). The angle θ has a value in radian that corresponds to 80 degrees. Numerics correspond to bare evolution of the unitary dynamics of the model, while analytical results are given by Eqs. (11), (17) and (18). The lines are a guide to the eye.

probability for our choice of the initial state is nonzero on site 0 only at even time steps. Consequently, we must choose the i.i.d. random variables τ_α as even numbers, as otherwise any projective measurement on the instantaneous state would yield null result. For our purpose, we make for the τ_α distribution p_τ two representative choices, namely, that of a discrete exponential distribution

$$\begin{aligned}
 p_\tau &= r(1-r)^{\tau/2-1}; \quad \tau = 2, 4, 6, \dots, \quad 0 < r < 1; \\
 \langle \tau \rangle &= \frac{2}{r}, \quad \text{Var}[\tau] = \frac{4(1-r)}{r^2},
 \end{aligned} \tag{20}$$

and that of a power-law distribution

$$\begin{aligned}
 p_\tau &= \frac{2^s}{\zeta(s)\tau^s}; \quad \tau = 2, 4, 6, \dots, \quad s > 1; \\
 \langle \tau \rangle &= \frac{2\zeta(s-1)}{\zeta(s)}, \quad s > 2; \quad \text{Var}[\tau] = \frac{4[\zeta(s)\zeta(s-2) - \zeta^2(s-1)]}{\zeta^2(s)}, \quad s > 3;
 \end{aligned} \tag{21}$$

where $\zeta(s) \equiv \sum_{n=1}^{\infty} 1/n^s$; $s > 1$ is the Riemann zeta function. Here, $\langle \tau \rangle$ denotes the mean of the distribution p_τ , while $\text{Var}[\tau]$ denotes its variance. All the aforementioned distributions satisfy the normalization $\sum_{\tau=2,4,6,\dots}^{\infty} p_\tau = 1$. The

exponential distribution (20) has all its moments, and in particular, the mean finite for all values of the parameter r . By contrast, the power-law distribution (21) has a finite mean only for $s > 2$ and a finite variance only for $s > 3$. Since any reasonable experimental set-up would allow measurements to be performed at random time intervals that have a finite average, as argued above, we will in this work consider only values of s larger than 2.

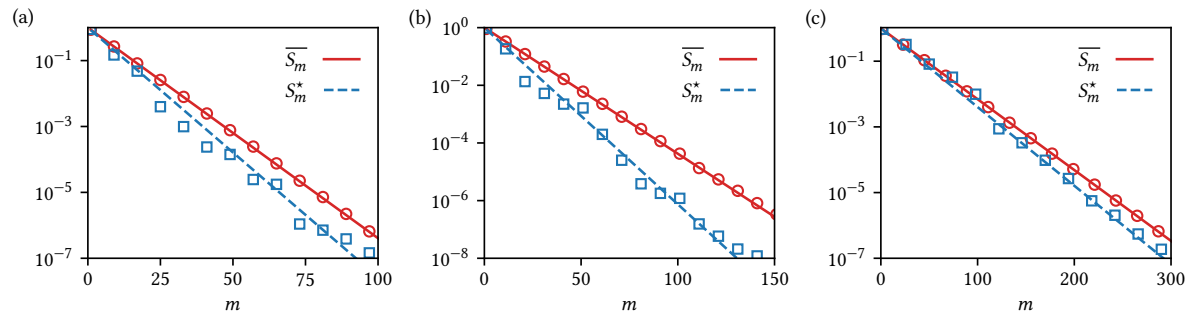


Figure 4. Average and typical survival probability for the QRW subject to instantaneous projective measurements at random times (**Scheme 1**). The plots correspond to the initial state (8) with $n_0 = 0$, $a = 1$, $b = i$ that is subject to repeated projective measurements at random times to the initial state and subsequent evolution with the projected component of the instantaneous state. Here, the time intervals τ_α between two consecutive measurements are i.i.d. random variables sampled from the exponential distribution (20) with $r = 0.5$ (panel (a)) and from the power-law distribution (21) with $s = 2.5$ (panel (b)) and $s = 3.5$ (panel (c)). The angle θ characterizing the QRW evolution operator C has the value in radian corresponding to 80 degrees. The system size is $N = 500$. In the plots, the points are based on results obtained from numerical implementation of the dynamics; while the average survival probability $\overline{S_m}$ involves averaging over 3000 realizations of the set $\{\tau_\alpha\}_{1 \leq \alpha \leq m}$, the typical survival probability S_m^* corresponds to results obtained in a typical realization of the τ_α 's. The lines in the plots correspond to analytical results given by Eqs. (30), (31), and (29).

In Fig. 4, we show in case of the evolution under **Scheme 1** our numerical results on the average survival probability $\overline{S_m}$ when averaged over typically hundreds of realizations $\{\tau_\alpha\}_{1 \leq \alpha \leq m}$ and the survival probability S_m^* obtained in a typical realization of the τ_α 's, both plotted as a function the m , the number of measurements. In the figure, panel (a) corresponds to τ_α 's distributed according to the exponential distribution (20) with $r = 0.5$, while panels (b) and (c) are for the power-law distribution (21) with s having values 2.5 and 3.5, respectively. The panels suggest for both the quantities $\overline{S_m}$ and S_m^* an exponential decay with m for large m .

We now present our results for **Scheme 2**. In order to contrast with those presented in Fig. 4 for **Scheme 1**, we use the same initial state. Figure 5 shows our numerical results on the average survival probability $\overline{S_m}$ and the typical survival probability S_m^* for the exponential distribution (20) with $r = 0.5$ (panels (a) and (d)), and for the power-law distribution (21) with $s = 2.5$ (panels (b) and (e)) and $s = 3.5$ (panels (c) and (f)). Based on our obtained results, we first summarize the behavior of $\overline{S_m}$.

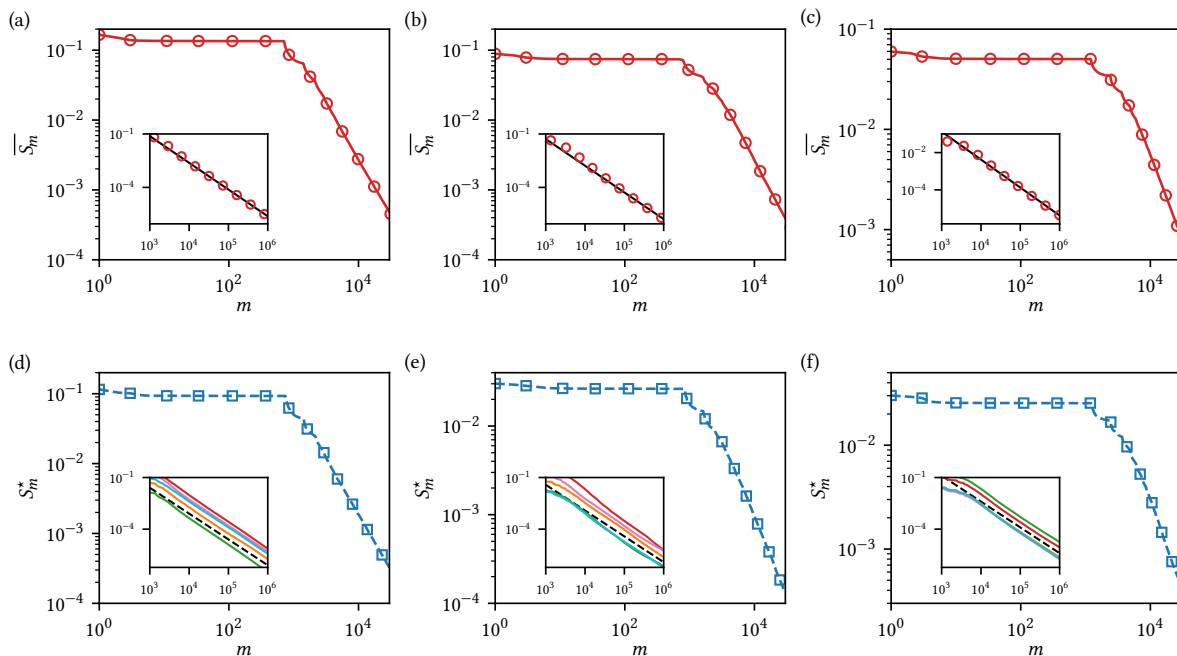


Figure 5. Average survival probability (panels (a) – (c)) and typical survival probability (panels (d) – (f)) for the QRW subject to instantaneous projective measurements at random times (**Scheme 2**). The plots correspond to the initial state (8) with $n_0 = 0$, $a = 1$, $b = i$ that is subject to repeated projective measurements at random times to the initial state and subsequent evolution with the leftover component of the instantaneous state after the measurement. Here, the time intervals τ_α between two consecutive measurements are i.i.d. random variables sampled from the exponential distribution (20) with $r = 0.5$ (panels (a) and (d)), and from the power-law distribution (21) with $s = 2.5$ (panels (b) and (e)) and $s = 3.5$ (panels (c) and (f)). The angle θ characterizing the QRW evolution operator C has the value in radian corresponding to 80 degrees. The system size is $N = 500$. In the main plots, the points are based on results obtained from numerical implementation of the dynamics; while the average survival probability \overline{S}_m involves averaging over 10 realizations (panel (a)), over 20 realizations (panel (b)), and over 10 realizations (panel (c)) of the set $\{\tau_\alpha\}_{1 \leq \alpha \leq m}$, the typical survival probability S_m^* corresponds to results obtained in a typical realization of the τ_α 's. The lines in the main plots correspond to those obtained from the semi-analytical approach described in the text, see Section 2.2.2. In the insets in the upper row, the points correspond to numerically-evaluated average survival probability, while the line represents an $m^{-3/2}$ behavior. In the insets in the lower row, the continuous lines correspond to numerically-evaluated survival probability for five typical realizations of $\{\tau_\alpha\}_{1 \leq \alpha \leq m}$, while the dashed line represents an $m^{-3/2}$ behavior. We conclude from the insets in both the upper and the lower row that the average as well as the typical survival probability behaves at large m as $m^{-3/2}$.

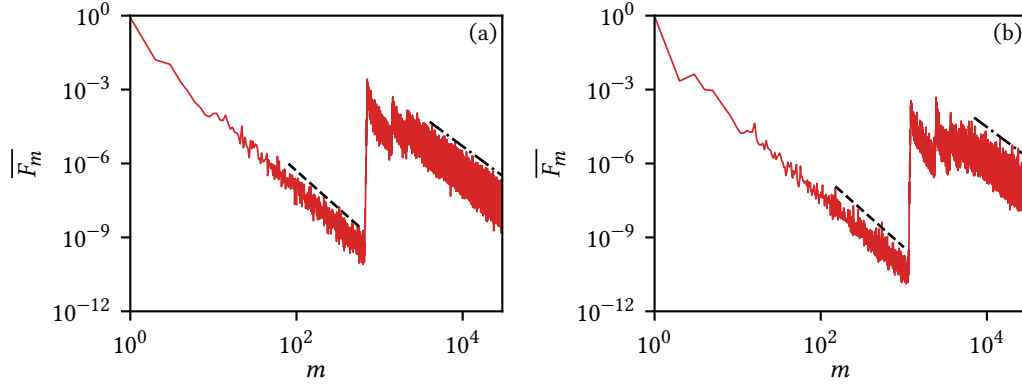


Figure 6. Average first-detection probability for the QRW model (**Scheme 2**). For panels (a) and (b), parameter values and number of averaging realizations are the same as in Figs. 5(a) and 5(c), respectively. As shown in the plots, one may observe two distinct behaviours $\sim m^{-3}$ (dashed line) and $\sim m^{-5/2}$ (dash-dotted line).

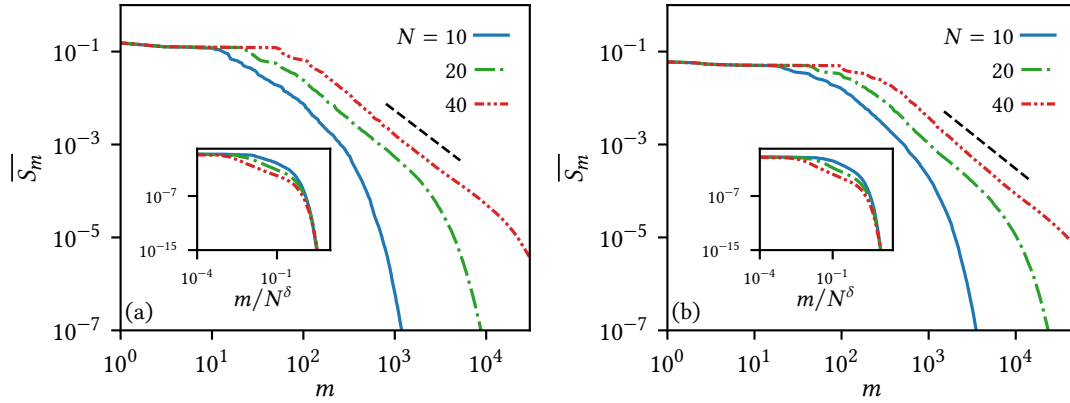


Figure 7. Average survival probability for the QRW model (**Scheme 2**). For panels (a) and (b), parameter values other than N and the number of averaging realizations are the same as in Figs. 5(a) and 5(c), respectively. The main plots show a crossover from a $m^{-3/2}$ -behaviour (dashed line) to an exponential tail over the characteristic value $m_2^*(N)$ of m ; the collapse of the data shown in the insets suggests the scaling (23).

- (i) There are two characteristic N -dependent m values, namely, $m_1^*(N)$ and $m_2^*(N)$, that characterize the behaviour of \overline{S}_m . While $m_1^*(N)$ scales linearly with N , the other scale $m_2^*(N)$ grows superlinearly with N .
- (ii) For $m < m_1^*(N)$ and large, one has $\overline{S}_m \sim m^{-2}$, implying thereby the behavior of the average first-detection probability as $\overline{F}_m \sim m^{-3}$, see Eq. (1) for the definition of F_m in terms of S_m .
- (iii) For m satisfying $m_1^*(N) \ll m < m_2^*(N)$, one has $\overline{S}_m \sim m^{-3/2}$, implying thereby the behavior of the average first-detection probability as $\overline{F}_m \sim m^{-5/2}$.
- (iv) For $m \gg m_2^*(N)$, one has an exponential decay of \overline{S}_m with m .
- (v) While the $m^{-3/2}$ -behavior of \overline{S}_m may already be observed in Fig. 5, in the insets of panels (a) – (c), in order to observe the m^{-2} -behaviour, it proves convenient to look

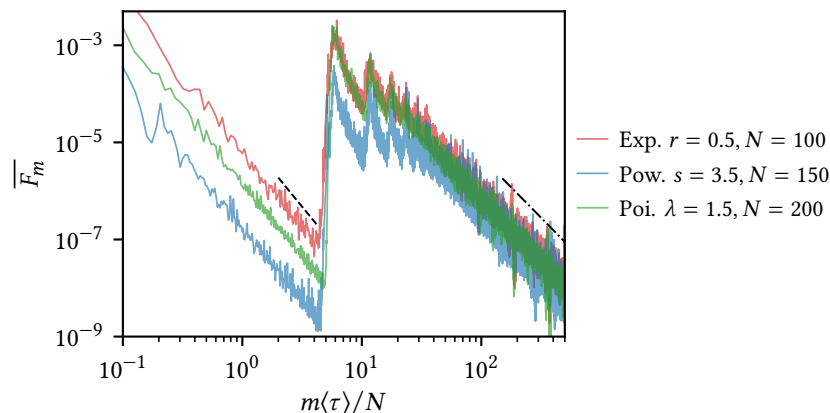


Figure 8. Average first-detection probability for the QRW model (**Scheme 2**) for the exponential distribution (20), the power-law distribution (21), and the Poisson distribution (25). Here, the parameters n_0 , a , b , and θ have the same values as in Fig. 5. The number of averaging realizations in all cases is 50. The parameter r for the exponential distribution and the parameter s for the power-law distribution have the same values as in Fig. 5, panels (a) and (c), respectively. For the data plotted for the Poisson distribution (25), we have $\lambda = 1.5$. The plot suggests the scaling depicted in Eq. (22).

at the plot of the corresponding \overline{F}_m , see Fig. 6, in which the two aforementioned distinct behaviours of m^{-3} and $m^{-5/2}$ may be clearly observed. The exponential decay of \overline{S}_m with m for $m \gg m_2^*(N)$ may be seen from Fig. 7. Note that since $m_2^*(N)$ grows superlinearly with N , in order to observe this exponential decay for the value of N used in Fig. 5, one has to obtain results for very large values of m , requiring computation for a prohibitively-long time. Hence, we use in Fig. 7 a smaller N than the one used in Fig. 5.

- (vi) That the characteristic scale $m_1^*(N)$ scales linearly with N may be deduced from Fig. 8, which indeed implies that

$$m_1^*(N) \sim \frac{N}{\langle\tau\rangle}, \quad (22)$$

where $\langle\tau\rangle$ is the average of the distribution p_τ .

- (vii) The superlinear scaling of $m_2^*(N)$ with N may be deduced from the insets of Fig. 7. We find:

$$m_2^*(N) \sim N^\delta; \quad \delta = 3.0. \quad (23)$$

In the above backdrop, we may mention that if one studies an infinite system (i.e., the limit $N \rightarrow \infty$), the scale $m_1^*(N)$ diverges, and one would observe the large- m behavior $\overline{S}_m \sim m^{-2}$ and $\overline{F}_m \sim m^{-3}$.

One may wonder about the robustness of all of the aforementioned behaviour with respect to distributions p_τ other than the exponential distribution (20) and the power-law distribution (21) that we have considered until now. To this end, we now

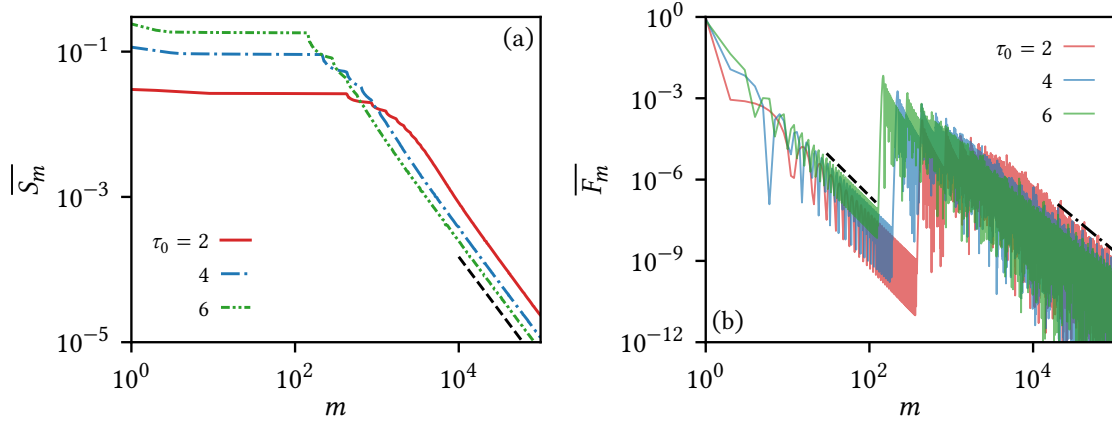


Figure 9. Average survival and first-detection probability for the QRW model (**Scheme 2**). Here, the parameters n_0 , a , b , and θ have the same values as in Fig. 5. Here, the time intervals τ_α between two consecutive measurements are i.i.d. random variables sampled from the distribution (24). The values of the parameter τ_0 are shown in the figure. The system size is $N = 150$. In panel (a), as shown in the plot, one may observe a behavior $\sim m^{-3/2}$ (dashed line), while in panel (b), two distinct behaviours $\sim m^{-3}$ (dashed line) and $\sim m^{-5/2}$ (dash-dotted line) may be seen. Note that since τ has only one allowed value, namely, τ_0 , it is redundant to use the overbar over S_m and F_m to denote their average values.

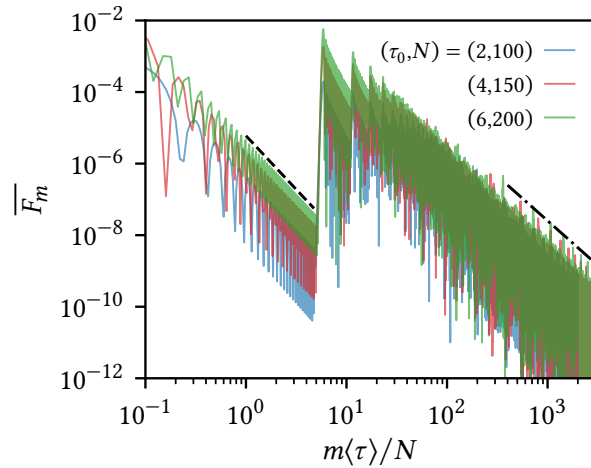


Figure 10. Average first-detection probability for the QRW model (**Scheme 2**). Parameter values and other details are the same as in Fig. 9. The plot suggests that the crossover from the $\sim m^{-3}$ -behaviour (dashed line) to the $\sim m^{-5/2}$ -behaviour (dash-dotted line) over the characteristic value $m_1^*(N)$ of m that follows the scaling (22). Note that since τ has only one allowed value, namely, τ_0 , it is redundant to use the overbar over F_m to denote its average.

demonstrate that the same behavior is also observed for two other distributions, namely, the case corresponding to measurements performed at regular time interval τ_0 :

$$p_\tau = \delta_{\tau, \tau_0}; \quad \tau = 2, 4, 6, \dots; \quad \tau_0 > 0; \quad \langle \tau \rangle = \tau_0, \quad \text{Var}[\tau] = 0, \quad (24)$$

and the Poisson distribution

$$p_\tau = \frac{e^{-\lambda} \lambda^{\tau/2-1}}{(\tau/2-1)!}; \quad \tau = 2, 4, 6, \dots; \quad \lambda > 0; \quad \langle \tau \rangle = 2(1 + \lambda), \quad \text{Var}[\tau] = 4\lambda, \quad (25)$$

as one varies the parameter λ that controls the width of the distribution p_τ , leading to a small (respectively, large) variance for small (respectively, large) λ . Results for the case of the delta-function distribution (24) are shown in Figs. 9 and 10. One may observe from these figures and in appropriate regimes the $m^{-3/2}$ behavior of \overline{S}_m , the m^{-3} behavior and the $m^{-5/2}$ behavior of \overline{F}_m , and the scaling of the crossover scale $m_1^*(N)$ according to Eq. (22). Since similar results are obtained for the case of the Poisson distribution (25), we do not present all the results here, excepting to show in Fig. 8 the scaling of $m_1^*(N)$ in accordance with Eq. (22).

So far we have discussed the behavior of the average quantities, but even the typical survival probability S_m^* and the typical first-detection probability F_m^* behave in a manner similar to their respective averages. Some representative plots are given in Fig. 5, panels (d) – (f), and in Fig. 11.

Before closing this part, the last issue that we discuss is the behavior of \overline{S}_m and \overline{F}_m for small $m \ll m_1^*(N)$. As it turns out, these quantities show oscillations in such a regime, with the oscillations becoming more pronounced as the distribution p_τ becomes more narrow. To show a representative result, we plot in Fig. 12 the quantity \overline{F}_m versus m for the case of the Poisson distribution (25) as one varies the parameter λ that controls the narrowness of the distribution. It is evident from the plot that with decrease of λ , oscillations in the behavior of \overline{F}_m become more pronounced. This feature is generic across the different p_τ 's that we considered (of course, for the delta-function distribution (24), the oscillations look most striking).

On the basis of the foregoing, we see a stark contrast between our obtained results on the survival probability under the two choices of the dynamics. It is our objective in the following to offer an analytical treatment of these results.

2.2.2. Analytical results In **Scheme 1**, we obtain $|\psi_m^{(a)}\rangle$ for arbitrary m as

$$|\psi_m^{(a)}\rangle = PU_m \dots PU_3 PU_2 PU_1 |\psi(0)\rangle. \quad (26)$$

From Eqs. (3), (2), and (26), we see that S_m may be expressed as

$$S_m = \prod_{\alpha=1}^m q(\tau_\alpha), \quad (27)$$

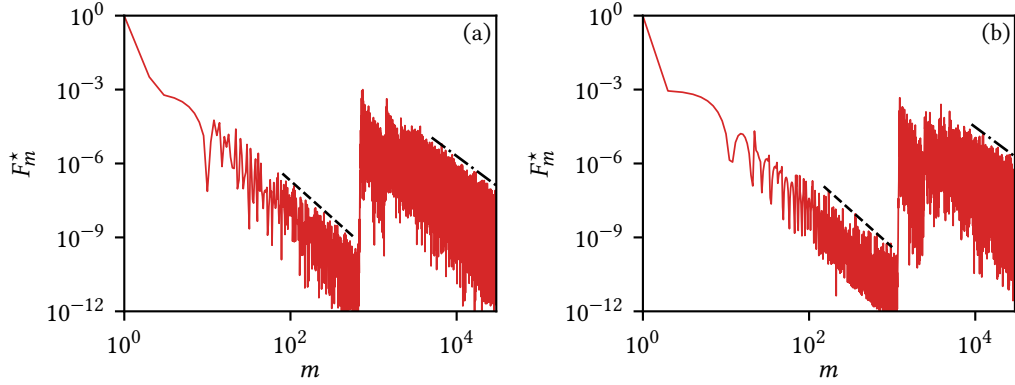


Figure 11. Typical first-detection probability for the QRW model (**Scheme 2**). For panels (a) and (b), parameter values are the same as in Figs. 5(a) and 5(c), respectively. As shown in the plots, one may observe two distinct behaviours $\sim m^{-3}$ (dashed line) and $\sim m^{-5/2}$ (dash-dotted line).

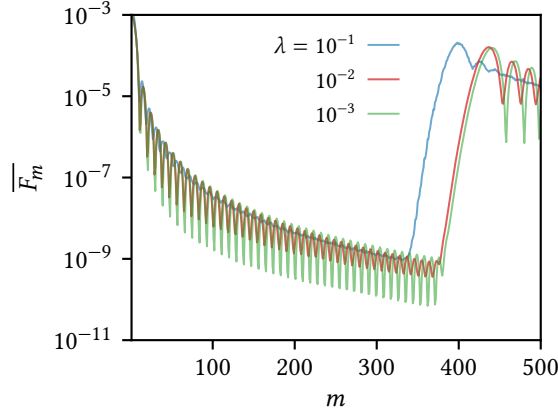


Figure 12. Average first-detection probability for the QRW model (**Scheme 2**) for the Poisson distribution (25) with different values of λ . Here, the parameters n_0 , a , b , and θ have the same values as in Fig. 5. The system size is $N = 150$, while the number of averaging realizations is 1000.

where the (quantum) probability $q(\tau_\alpha)$ is given by

$$q(\tau_\alpha) \equiv |\langle \psi(0) | U_\alpha | \psi(0) \rangle|^2 \quad (28)$$

$$= \frac{1}{|a|^2 + |b|^2} |a^* \Psi_u(n_0, \tau_\alpha) + b^* \Psi_d(n_0, \tau_\alpha)|^2, \quad (29)$$

with $\Psi_u(n_0, \tau_\alpha)$ and $\Psi_d(n_0, \tau_\alpha)$ given by Eqs. (17) and (18). Note that $q(\tau)$ is nothing but the probability for the walker to be found in the initial state $|\psi(0)\rangle$ after evolution for time τ . Using Eq. (27), one obtains the average survival probability as

$$\overline{S_m} = \prod_{i=1}^m \left(\sum_{\tau} p_{\tau} q(\tau) \right) = \exp \left(m \log \sum_{\tau} p_{\tau} q(\tau) \right). \quad (30)$$

As shown in Appendix A, the most probable value of the survival probability S_m^* is obtained as

$$S_m^* = \exp \left(m \sum_{\tau} p_{\tau} \log q(\tau) \right). \quad (31)$$

Using the Jensen's inequality $\overline{\exp(x)} \geq \exp(\bar{x})$, we obtain that

$$\overline{S_m} \geq S_m^*, \quad (32)$$

with the equality holding only when there is no randomness in τ , that is, when τ can take on only a single value: $p_{\tau} = \delta_{\tau, \tau_0}$, with $\tau_0 > 0$. On performing a large number m of projective measurements, the value of the survival probability to remain in the initial state that is measured in a single experimental run will equal S_m^* in the limit $m \rightarrow \infty$. On the other hand, averaging the survival probability over a large (ideally infinite) number of experimental runs would yield the value $\overline{S_m}$.

The theoretical results are compared against those obtained in numerical implementation of the **Scheme 1** dynamics in Fig. 4. In this figure, the continuous lines in red obtained from Eq. (30) show the behavior of $\overline{S_m}$, while the blue-dashed lines obtained from Eq. (31) depict that of S_m^* . We see from the figure a very good match between theoretical and numerical results for the average survival probability, whereas the numerical results for the most probable survival probability fluctuate around the theoretical estimate as expected.

In **Scheme 2**, we obtain $|\psi_m^{(a)}\rangle$ for arbitrary m as

$$|\psi_m^{(a)}\rangle = \tilde{P}U_m \dots \tilde{P}U_3 \tilde{P}U_2 \tilde{P}U_1 |\psi(0)\rangle. \quad (33)$$

In this scheme, to find an analytical closed form of $\overline{S_m}$ and S_m^* is non-trivial, as we explain below. Consequently, we rely on a semi-analytical approach that involves implementation of the following four steps:

- (i) For a given choice of a , b , and n_0 specifying the initial state $|\psi(0)\rangle$ in Eq. (8), we first obtain the vector $|\Psi(n, 0)\rangle$ by using Eqs. (10) and (12). Then, we implement the discrete Fourier transform given by $|\tilde{\Psi}(k, 0)\rangle = \sum_n |\Psi(n, 0)\rangle e^{i2\pi kn/N}$.
- (ii) Subsequently, we use Eq. (14) to obtain $|\tilde{\Psi}(k, \tau_1)\rangle$ as the result of dynamical evolution for a random time τ_1 sampled according to either the exponential distribution (20) or the power-law distribution (21), and with $|\tilde{\Psi}(k, 0)\rangle$ as the initial condition. At the end of the evolution, one has the set $\{|\tilde{\Psi}(k, \tau_1)\rangle\}$.
- (iii) Next, we perform inverse discrete Fourier transform of the set $\{|\tilde{\Psi}(k, \tau_1)\rangle\}$ to obtain the set $\{|\Psi(n, \tau_1)\rangle\}$. To implement a projective measurement at the end of evolution for time τ_1 and obtaining the corresponding leftover component of the state, we first obtain the state $|\psi(\tau_1)\rangle$ by using the obtained values of the elements of $\{|\Psi(n, \tau_1)\rangle\}$ in Eq. (10), and then compute the difference $|\psi(\tau_1)\rangle - |\psi(0)\rangle\langle\psi(0)|\psi(\tau_1)\rangle$, which yields the state $|\psi_1^{(a)}\rangle$.

- (iv) Steps 1–3 are applied in turn to the leftover component of the state corresponding to last projection; $m \geq 1$ number of repetitions would generate the leftover component of the instantaneous state after m projections, and this allows us to obtain the survival probability S_m for a given realization $\{\tau_\alpha\}_{1 \leq \alpha \leq m}$ of the dynamics.

The method is semi-analytical in the sense that while the dynamical evolution in the Fourier space follows the exact solution (14), inverse Fourier transform to obtain $|\Psi(n, \tau)\rangle$ is performed numerically. The semi-analytical results for the average and the typical survival probability are compared in Fig. 5 against numerical results, demonstrating a very good match.

We remark that in **Scheme 1**, each time a projective measurement is made, the dynamical evolution starts afresh from a state that is just the initial state multiplied by a complex number (e.g., the state for subsequent dynamical evolution after say the first measurement is $|\psi_1^{(a)}\rangle = \langle\psi(0)|\psi(\tau_1)\rangle|\psi(0)\rangle$). Consequently, the survival probability S_m is a product of the quantum probabilities $q(\tau_\alpha)$ over different times τ_α , see Eq. (27). This is however not the case in **Scheme 2**, and this defies the survival probability S_m to be written as a product of probabilities for different τ_α 's and consequently, a straightforward analytical estimate of the average and the typical survival probability for **Scheme 2**.

3. Tight-binding model (TBM)

3.1. Model and site occupation probability

The tight-binding model (TBM) that we now study involves quantum evolution of a particle on a one-dimensional lattice that we consider here to be of N sites with periodic boundary conditions. The dynamics in continuous time is generated by the Hamiltonian [7, 8]

$$H = -\gamma \sum_{j=0}^{N-1} (|j+1\rangle\langle j| + |j\rangle\langle j+1|); \quad |N\rangle = |0\rangle. \quad (34)$$

Here, $\gamma > 0$ is a real parameter, while the index j denotes the lattice sites. Let $\psi_{n,n_0}(t) = \langle n|\psi(t)\rangle$, with $n = 0, 1, 2, \dots, N-1$ be the probability amplitude to find the particle on site n at time t while starting from site n_0 at time $t = 0$, with the normalization $\sum_{n=0}^{N-1} |\psi_{n,n_0}(t)|^2 = 1 \forall t$. From the evolution equation $|\psi(t + \Delta t)\rangle = \exp(-iH\Delta t)|\psi(t)\rangle$; $|\psi(0)\rangle = |n_0\rangle$, one obtains the time evolution of $\psi_{n,n_0}(t)$ in a small time interval Δt as

$$\psi_{n,n_0}(t + \Delta t) = \sum_{j=0}^{N-1} \langle n|e^{-iH\Delta t}|j\rangle \psi_{j,n_0}(t). \quad (35)$$

Expanding in powers of Δt the right hand side of the above equation and then taking the limit of continuous time, $\Delta t \rightarrow 0$, one obtains the evolution $\partial\psi_{n,n_0}(t)/\partial t =$

$-i \sum_{j=0}^{N-1} \langle n|H|j \rangle \psi_{j,n_0}(t)$. Equation (34) gives $\langle j|H|k \rangle = -\gamma (\delta_{j,k-1} + \delta_{j,k+1})$, yielding

$$\frac{\partial \psi_{n,n_0}(t)}{\partial t} = i\gamma (\psi_{n-1,n_0}(t) + \psi_{n+1,n_0}(t)). \quad (36)$$

In order to solve Eq. (36) for $\psi_{n,n_0}(t)$, we perform discrete Fourier transform of the set $\{\psi_{n,n_0}(t)\}_{0 \leq n \leq N-1}$, given by the set $\{\widehat{\psi}_{q|n_0}(t)\}_{0 \leq q \leq N-1}$, with $\widehat{\psi}_{q|n_0}(t) = \sum_{j=0}^{N-1} \psi_{j,n_0}(t) \exp(-i2\pi j q/N)$; $\psi_{j,n_0}(t) = (1/N) \sum_{q=0}^{N-1} \widehat{\psi}_{q|n_0}(t) \exp(i2\pi j q/N)$. From Eq. (36), one then obtains

$$\frac{\partial \widehat{\psi}_{q|n_0}(t)}{\partial t} = 2i\gamma \cos\left(\frac{2\pi q}{N}\right) \widehat{\psi}_{q|n_0}(t). \quad (37)$$

Subject to the initial condition $\psi_{n,n_0}(0) = \delta_{n,n_0}$ implying $\widehat{\psi}_{q|n_0}(0) = \exp(-i2\pi n_0 q/N)$, Eq. (37) has the solution $\widehat{\psi}_{q|n_0}(t) = \exp(i2\gamma t \cos(2\pi q/N) - i2\pi n_0 q/N)$, inverting which yields

$$\psi_{j,n_0}(t) = \frac{1}{N} \sum_{q=0}^{N-1} e^{i2\gamma t \cos(2\pi q/N) + i2\pi q(j-n_0)/N}. \quad (38)$$

It is easily checked that $\sum_{j=0}^{N-1} |\psi_{j,n_0}(t)|^2 = 1$, as required. In particular, starting with the particle on site n_0 , we may ask for the probability $P_n(t)$ to be on site n at time t , the so-called site occupation probability. It is given by

$$P_n(t) = |\psi_{n,n_0}(t)|^2 = \left| \frac{1}{N} \sum_{q=0}^{N-1} e^{i2\gamma t \cos(2\pi q/N) + i2\pi q(n-n_0)/N} \right|^2. \quad (39)$$

In Fig. 13, we show a comparison between numerical results and theory, demonstrating a perfect match. In the figure, numerics correspond to bare evolution of the unitary dynamics of the model, while analytical results are given by Eq. (39).

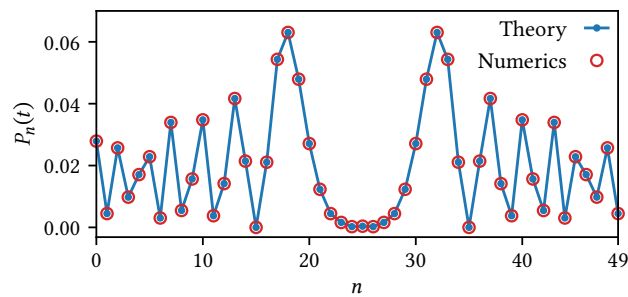


Figure 13. Site occupation probability $P_n(t)$ in the TBM on a one-dimensional periodic lattice of N sites and at time $t = 10$, while starting from initial site $n_0 = 0$. Here, we have $N = 50, \gamma = 1$. Numerics correspond to bare evolution of the unitary dynamics of the model, while analytical results are given by Eq. (39). The line is a guide to the eye.

3.2. Random projective measurements and survival probability

3.2.1. Numerical results Here, we report numerical results on the average and the typical survival probability for the TBM subject to projective measurements at random times. A typical time evolution of the system is shown in Fig. 1. The initial state corresponds to the particle located on site n_0 (thus, $|\psi(0)\rangle = |n_0\rangle$), and as in the case of the QRW reported above, we consider the projective measurement to be involving projection to the initial state n_0 implemented by the projection operator $P = |n_0\rangle\langle n_0|$. Here, the random variable τ between two successive measurements, now a continuous variable, is taken to be distributed according to either an exponential distribution:

$$p(\tau) = r \exp(-r\tau); \quad \tau \in [0, \infty), \quad r > 0; \quad \langle \tau \rangle = \frac{1}{r}, \quad \text{Var}[\tau] = \frac{1}{r^2}, \quad (40)$$

or a power-law distribution:

$$p(\tau) = \frac{\alpha}{\tau_{\text{ch}}(\tau/\tau_{\text{ch}})^{1+\alpha}}; \quad \tau \in [\tau_{\text{ch}}, \infty), \quad \alpha > 0; \quad (41)$$

$$\langle \tau \rangle = \frac{\tau_{\text{ch}} \alpha}{\alpha - 1}, \quad \alpha > 1; \quad \text{Var}[\tau] = \frac{\tau_{\text{ch}}^2 \alpha}{(\alpha - 2)(\alpha - 1)^2}, \quad \alpha > 2.$$

In Eq. (41), the parameter $\tau_{\text{ch}} > 0$ sets the lower cut-off scale. The exponential distribution (40) has a finite mean for all values of r . On the other hand, the power-law distribution (41) has a finite mean only for $\alpha > 1$ and a finite variance only for $\alpha > 2$, and since we would like in the view of discussions presented in Section 2.2 to have the τ_α 's to have a finite average, we will in the following consider values of α to be larger than 1.

Figure 14 shows in case of the evolution under **Scheme 1** our numerical results on the average survival probability \overline{S}_m and the typical survival probability S_m^* , both plotted as a function the m , the number of measurements. In the figure, panel (a) corresponds to the exponential distribution (40) for the τ with $r = 2$, while panels (b) and (c) are for the power-law distribution (41) with α having values 2.5 and 3.5, respectively. The panels suggest for both the quantities \overline{S}_m and S_m^* an exponential decay with m for large m .

As regards **Scheme 2** dynamics, the behavior of both the average and the typical value of the survival and the first-detection probability is identical to what we reported for the QRW, see Section 2.2.1. The statement holds not just for the exponential distribution (40) and the power-law distribution (41), but also for the delta-function distribution corresponding to measurements performed at regular intervals:

$$p(\tau) = \delta(\tau - \tau_0); \quad \tau_0 > 0; \quad \langle \tau \rangle = \tau_0, \quad \text{Var}[\tau] = 0, \quad (42)$$

and for the half-normal distribution:

$$p(\tau) = \sqrt{\frac{2}{\pi\sigma^2}} \exp\left[-\frac{(\tau - \tau_{\text{hn}})^2}{2\sigma^2}\right]; \quad \tau \in [\tau_{\text{hn}}, \infty), \quad \sigma > 0; \quad (43)$$

$$\langle \tau \rangle = \tau_{\text{hn}} + \sigma\sqrt{\frac{2}{\pi}}, \quad \text{Var}[\tau] = \sigma^2 \left(1 - \frac{2}{\pi}\right),$$

in which the quantity τ_{hn} sets the lower limit of τ . Indeed, as shown in Figs. 15 and 16, one observes in $\overline{S_m}$ and $\overline{F_m}$ the occurrence of the $m^{-3/2}$ behaviour in the former and of m^{-3} and $m^{-5/2}$ behavior in the latter. The crossover between the m^{-3} and the $m^{-5/2}$ behavior takes place over the characteristic value $m_1^*(N)$ that satisfies the scaling (22), as implied by the results in Fig. 18. The existence of the characteristic value $m_2^*(N)$ satisfying the scaling (23) may be seen in Fig. 17. The results for the delta-function distribution (42) are included in Figs. 19 and 20, while those for the typical survival probability in the case of the exponential distribution (40) and (41) are shown in Fig. 21. The existence of oscillations in the behavior of $\overline{F_m}$ at small $m < m_1^*(N)$ that become more pronounced as the distribution $p(\tau)$ of the time interval between successive measurements is shown for the case of the half-normal distribution (43) in Fig. 22. Let us remark that our results summarized above hold for finite N , while if one studies an infinite system (i.e., the limit $N \rightarrow \infty$), the scale $m_1^*(N)$ diverges, and one observes the large- m behavior $\overline{S_m} \sim m^{-2}$ and $\overline{F_m} \sim m^{-3}$.

On the basis of the foregoing, we remark that similar to the results for the QRW reported in Section 2.2, we see a stark contrast in the behavior of the survival probability under **Scheme 1** and **Scheme 2** of the measurement dynamics in the case of the TBM.

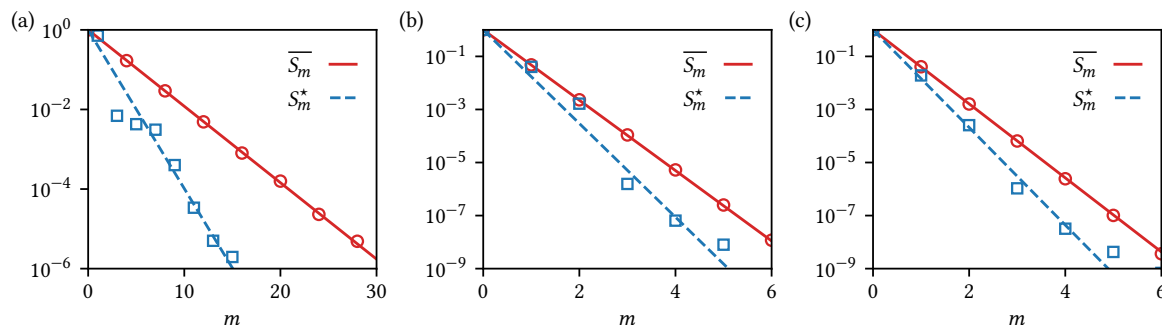


Figure 14. Average and typical survival probability for the TBM subject to instantaneous projective measurements at random times (**Scheme 1**). The plots correspond to the initial state $|0\rangle$ (particle located on site $n_0 = 0$) that is subject to repeated projective measurements at random times to the initial state and subsequent evolution with the projected component of the instantaneous state. Here, the time intervals τ_α between two consecutive measurements are i.i.d. random variables sampled from the exponential distribution (40) with $r = 2.0$ (panel (a)) and from the power-law distribution (41) with $\tau_{\text{ch}} = 1$ and $\alpha = 2.5$ (panel (b)) and $\alpha = 3.5$ (panel (c)). The system size is $N = 200$, while we have taken $\gamma = 1$. In the plots, the points are based on results obtained from numerical implementation of the dynamics; while the average survival probability $\overline{S_m}$ involves averaging 10^4 realizations of the set $\{\tau_\alpha\}_{1 \leq \alpha \leq m}$, the typical survival probability S_m^* corresponds to results obtained in a typical realization of the τ_α 's. The lines in the plots correspond to analytical results given by Eqs. (44) and (45).

In Refs. [13, 14, 19, 24], study of **Scheme 2** dynamics of the TBM, Eq. (34), was carried out for the case where the particle is projected to a state that is in general different from the initial state. More precisely, in Refs. [13, 14], the initial location of

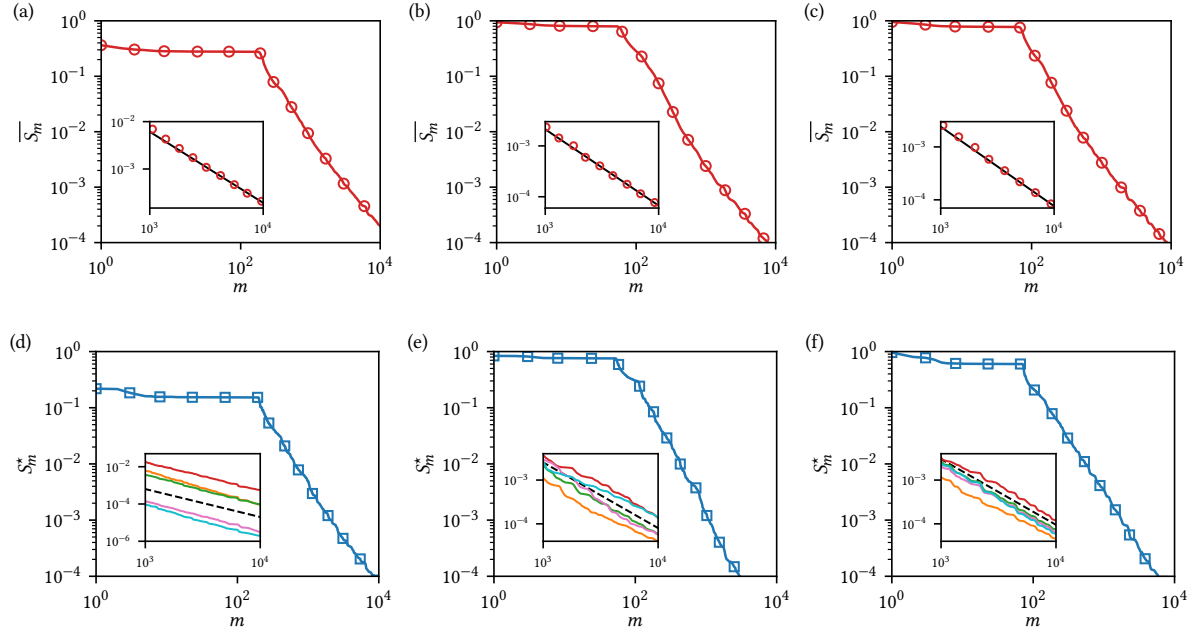


Figure 15. Average survival probability (panels (a) – (c)) and typical survival probability (panels (d) – (f)) for the TBM subject to instantaneous projective measurements at random times (**Scheme 2**). The plots correspond to the initial state $|0\rangle$ (particle located on site $n_0 = 0$) that is subject to repeated projective measurements at random times to the initial state and subsequent evolution with the leftover component of the instantaneous state after the measurement. Here, the time intervals τ_α between two consecutive measurements are i.i.d. random variables sampled from the exponential distribution (40) with $r = 2$ (panels (a) and (d)), and from the power-law distribution (41) with $\tau_{\text{ch}} = 1$ and $\alpha = 2.5$ (panels (b) and (e)) and $\alpha = 3.5$ (panels (c) and (f)). The system size is $N = 200$, while we have taken $\gamma = 1$. In the main plots, the points are based on results obtained from numerical implementation of the dynamics; while the average survival probability $\overline{S_m}$ involves averaging over 25 realizations of the set $\{\tau_\alpha\}_{1 \leq \alpha \leq m}$, the typical survival probability S_m^* corresponds to results obtained in a typical realization of the τ_α 's. The lines in the main plots correspond to those obtained from the semi-analytical approach described in the text, see Section 3.2.2. In the insets in the upper row, the points correspond to numerically-evaluated average survival probability, while the line represents an $m^{-3/2}$ behavior. In the insets in the lower row, the continuous lines correspond to numerically-evaluated survival probability for five typical realizations of $\{\tau_\alpha\}_{1 \leq \alpha \leq m}$, while the dashed line represents an $m^{-3/2}$ behavior. We conclude from the insets in both the upper and the lower row that the average as well as the typical survival probability behaves at large m as $m^{-3/2}$.

the particle is taken to be site l (thus, the initial state of the particle is $|l\rangle$), while the state to which the instantaneous state of the particle is repeatedly projected to is taken to be $|N\rangle$ (thus, the projection operator is $|N\rangle\langle N|$, and corresponds to measurements being made by a detector placed on site N of the lattice). An important difference with respect to our work is that in these set of work, projective measurements were considered to be taking place at regular intervals of length τ , as opposed to stochastic τ considered in our work. In these work, it was shown analytically that for large even N and large

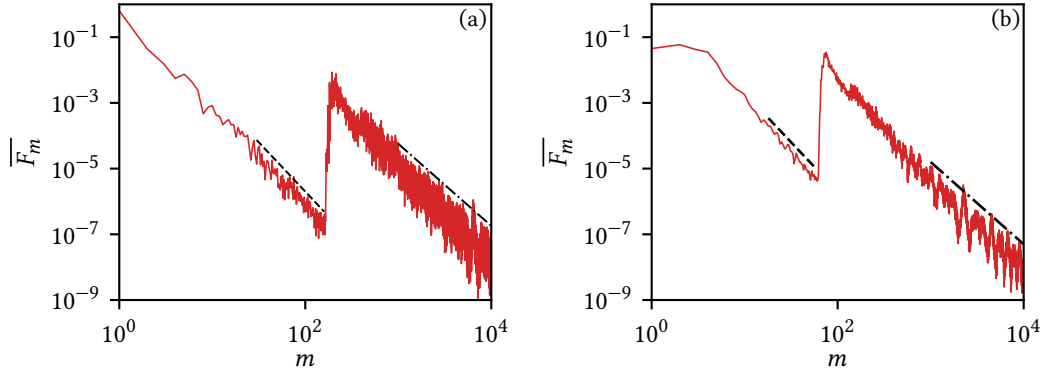


Figure 16. Average first-detection probability for the TBM (**Scheme 2**). For panels (a) and (b), parameter values and number of averaging realizations are the same as in Figs. 15(a) and 15(c), respectively. As shown in the plots, one may observe two distinct behaviours $\sim m^{-3}$ (dashed line) and $\sim m^{-5/2}$ (dash-dotted line).

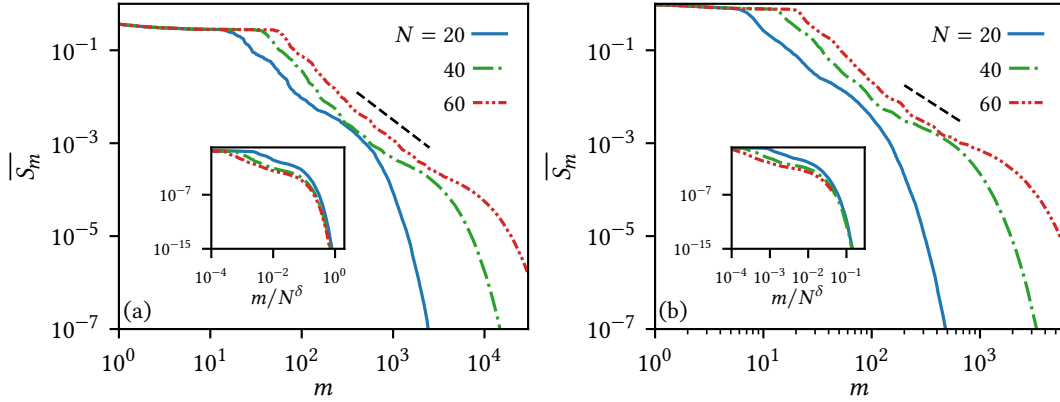


Figure 17. Average survival probability for the TBM (**Scheme 2**). For panels (a) and (b), parameter values other than N and the number of averaging realizations are the same as in Figs. 15(a) and 15(c), respectively. The main plots show a crossover from a $m^{-3/2}$ -behaviour (dashed line) to an exponential tail over the characteristic value $m_2^*(N)$ of m ; the collapse of the data shown in the insets suggests the scaling (23).

$m\tau^2/N$, the survival probability S_m decays as $m^{-3/2}$ when the separation between sites l and N , measured along the shortest path on the one-dimensional lattice, is of order 1 and as $m^{-1/2}$ when the separation is of order N . It was also revealed for even N that the survival probability decays to a nonzero constant equal to $1/2$ when the initial location is $l \neq N/2, N$ and to zero for $l = N/2, N$. In our case of stochastic measurements, we also observe the $m^{-3/2}$ -decay, and the probability decays to zero. Our results thus serve as an extension of the behavior $\sim m^{-3/2}$ of the survival probability reported in Ref. [13] to the case when the measurements are done not at regular but at random intervals distributed according to a wide class of distribution functions: exponential, power law, and half-normal for several values of the associated variance. The existence of the scales $m_1^*(N)$ and $m_2^*(N)$ has been discussed in Ref. [19] for the case of measurements at regular intervals.

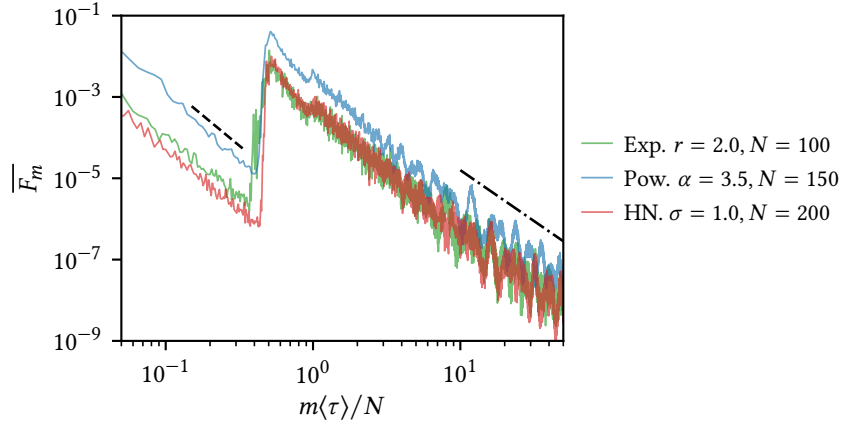


Figure 18. Average first-detection probability for the TBM (**Scheme 2**) for the exponential distribution (40), the power-law distribution (41), and the half-normal distribution (43). Here, the parameters n_0 and γ have the same values as in Fig. 15. The number of averaging realizations in all cases is 50. The parameter r for the exponential distribution and the parameters α and τ_{ch} for the power-law distribution have the same values as in Fig. 15, panels (a) and (c), respectively. For the data plotted for the half-normal distribution (43), we have $\tau_{\text{hn}} = 0.0$ and $\sigma = 1.0$. The plot suggests the scaling depicted in Eq. (22).

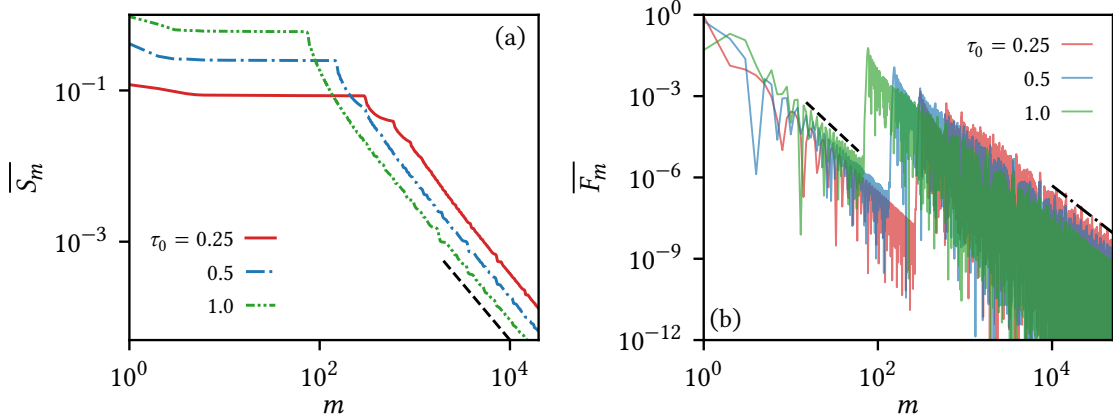


Figure 19. Average survival and first-detection probability for the TBM (**Scheme 2**). Here, the parameters n_0 and γ have the same values as in Fig. 15. Here, the time intervals τ_α between two consecutive measurements are i.i.d. random variables sampled from the distribution (42). The values of the parameter τ_0 are shown in the figure. The system size is $N = 150$. In panel (a), as shown in the plot, one may observe a behavior $\sim m^{-3/2}$ (dashed line), while in panel (b), two distinct behaviours $\sim m^{-3}$ (dashed line) and $\sim m^{-5/2}$ (dash-dotted line) may be seen. Note that since τ has only one allowed value, namely, τ_0 , it is redundant to use the overbar over S_m and F_m to denote their average values.

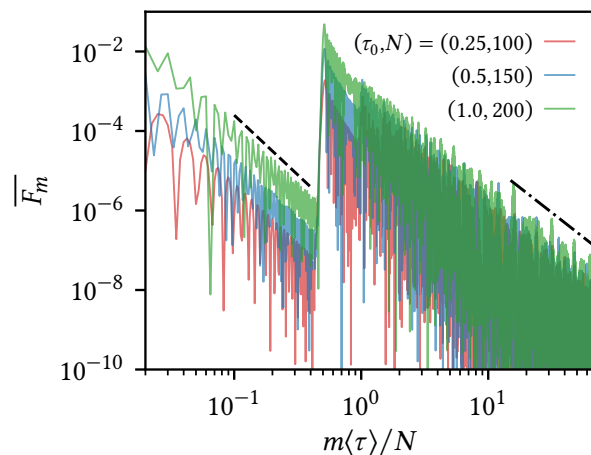


Figure 20. Average first-detection probability for the TBM (**Scheme 2**). Parameter values and other details are the same as in Fig. 19. The plot suggests that the crossover from the $\sim m^{-3}$ -behaviour (dashed line) to the $\sim m^{-5/2}$ -behaviour (dash-dotted line) over the characteristic value $m_1^*(N)$ of m that follows the scaling (22). Note that since τ has only one allowed value, namely, τ_0 , it is redundant to use the overbar over F_m to denote its average.

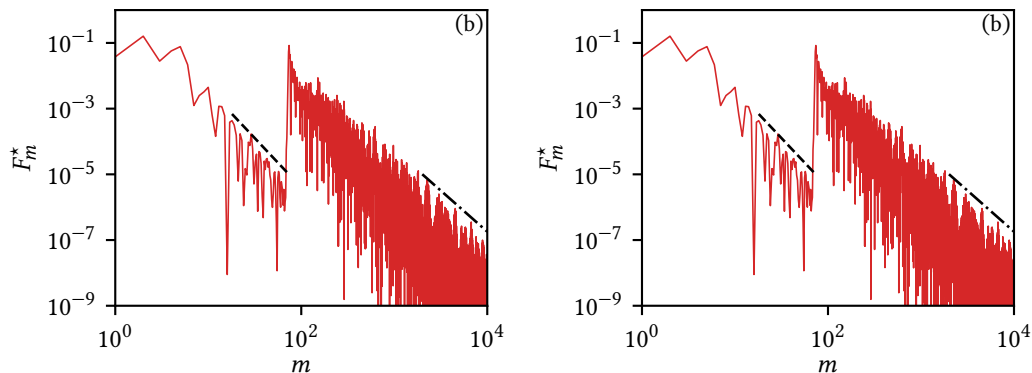


Figure 21. Typical first-detection probability for the TBM (**Scheme 2**). For panels (a) and (b), parameter values are the same as in Figs. 15(a) and 15(c), respectively. As shown in the plots, one may observe two distinct behaviours $\sim m^{-3}$ (dashed line) and $\sim m^{-5/2}$ (dash-dotted line).

A relevant study of the TBM subject to repeated projective measurements at regular time intervals of length τ , with dynamical evolution following **Scheme 2**, was pursued in Refs. [15, 16]. In these work, a quantum renewal equation approach was introduced to obtain the first detection probability F_m , namely, the probability that a quantum particle that is subject to projective measurements to a given site gets detected at the given site at time $m\tau$ for the first time. For the TBM defined on the infinite line, the probability of first detection was shown to exhibit a variety of rich behavior including, e.g., a decay as m^{-3} , in stark contrast to the $m^{-3/2}$ decay observed in the related system of classical Brownian motion. For the same dynamical setup, it was revealed in Ref. [17] that the first detection depends quite sensitively on the distance

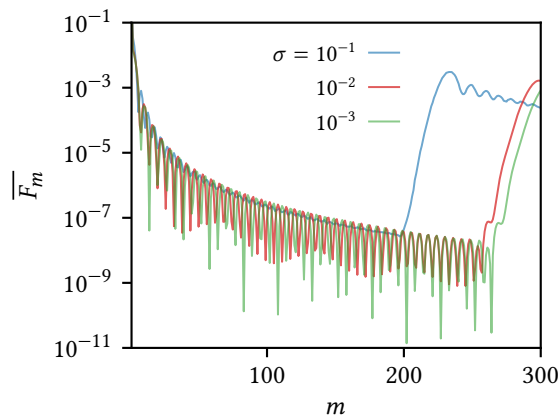


Figure 22. Average first-detection probability for the TBM (**Scheme 2**) for the half-normal distribution (43) with $\tau_{\text{hm}} = 0.25$ and different values of σ . Here, the parameters n_0 and γ have the same values as in Fig. 15. The system size is $N = 150$, while the number of averaging realizations is 500.

between the detector and the initial location of the particle and on τ , exhibiting scaling and nonanalytical behaviours in appropriate regimes. In Ref. [18], considering the **Scheme 2** of dynamics with measurements at regular intervals of equal length τ , the authors addressed the influence of the symmetries of a system on the total detection probability P_{det} , i.e., the probability to eventually detect the particle after an arbitrary number of detection attempts. It was demonstrated that this total detection probability is less than unity in symmetric systems, where one may find initial states, the so-called dark states, that are shielded from the detector by means of destructive interference. Reference [20] investigated under **Scheme 2** and considering measurements after every fixed time interval τ the effect of employing a moving detector on the first detection probability. For the TBM on the infinite line, it was shown that the system exhibits a dynamical phase transition at a critical τ , from a state where the probability of detection decreases exponentially in time and the total detection probability is very small, to one exhibiting a power-law decay and a significantly higher total detection probability. The average first detected return time, under **Scheme 2** of dynamics with measurements at every fixed interval of length τ , is known to be quantized, while the return time, a random variable, is known to exhibit huge fluctuations in appropriate regimes. In this backdrop, the work [21] derived explicit expressions for the variance of the return time, together with a classification scheme of the diverging variance based on different underlying physical effects. Reference [22] considered **Scheme 2** and measurements after fixed time intervals of length τ to study the total probability P_{det} in some target state, for example, on the node of a graph after one has made an arbitrary number of detection attempts. An explicit formula for P_{det} in terms of the energy eigenstates of the underlying system was derived, which was found to be generically τ -independent. The work is noteworthy in employing the formalism of the paper to obtain a simple upper bound for P_{det} . While the total detection probability P_{det} in classical random

walks is unity, the same for a quantum walker, with detection in some state $|d\rangle$, may for certain initial states $|\psi_{\text{in}}\rangle$ take a value smaller than unity. In Refs. [23, 25], the authors derived universal bounds for the quantum total detection probability, under **Scheme 2** of dynamics with measurements after every fixed interval of time equal to τ . It was shown that the deviation $\Delta P \equiv P_{\text{det}} - |\langle \psi_{\text{in}} | d \rangle|^2$ satisfies the inequality $\Delta P \text{Var}[H]_d \geq |\langle d | [H, D] | \psi_{\text{in}} \rangle|^2$, where $D = |d\rangle\langle d|$ is the measurement operator and $\text{Var}[H]$ measures energy fluctuations in state $|d\rangle$. Reference [26] studied by considering **Scheme 2** of dynamics the effect of conditional null measurements, done at equal intervals of time of length τ , on a quantum system and displayed a wide variety of rich behavior, e.g., for systems with built-in symmetry and a degenerate energy spectrum, the null measurements are found to dynamically select the degenerate energy levels, while the non-degenerate levels are effectively wiped out by the measurements.

In the above backdrop, we remark that our results reported in this work are complementary to those reported in Refs. [13, 14, 15, 16, 17, 18, 19, 20, 21, 22, 23, 24, 25, 26] because of the very different dynamical set-ups (regular τ) considered in these work with respect to ours (stochastic τ). The only exception to the above set of work that considered stochastic τ in the setting of the TBM with periodic boundary conditions is Ref. [27]. This work dealt with **Scheme 2** of dynamics, with the gap between consecutive measurements being independent and identically-distributed random variables τ distributed according to a given distribution $\rho(\tau)$. It was shown that for all $\rho(\tau)$ and finite-dimensional Hamiltonians, the mean detection time is equal to the mean attempt number multiplied by the mean time interval between detection attempts. Nevertheless, the issues and results that we report on in this work do not have overlap with this reference either. Let us remark that for the case of measurements at regular intervals, our results that in the limit $N \rightarrow \infty$, one would observe the behavior $F_m \sim m^{-3}$ is fully consistent with what is reported in Ref. [16].

3.2.2. Analytical results For **Scheme 1**, on using the continuous- τ equivalent of Eqs. (30) and (31), one may obtain the average and the typical survival probability for the TBM subject to projective measurements at random times intervals τ distributed according to the exponential and the power-law distribution, Eqs. (40) and (41), respectively. One has

$$\begin{aligned} \overline{S}_m &= \exp \left(m \log \int d\tau p(\tau) q(\tau) \right), \\ S_m^* &= \exp \left(m \int d\tau p(\tau) \log q(\tau) \right). \end{aligned} \quad (44)$$

In this case, $q(\tau)$, see Eq. (28), is nothing but the probability to be on site n_0 after time τ while starting from the same site, and is therefore obtained from Eq. (39) as

$$q(\tau) = |\psi_{n_0, n_0}(\tau)|^2 = \left| \frac{1}{N} \sum_{q=0}^{N-1} e^{i2\gamma\tau \cos(2\pi q/N)} \right|^2. \quad (45)$$

The theoretical results so obtained are compared in Fig. 14 against those obtained in numerical implementation of the **Scheme 1** dynamics. We see from the figure a very good match of the average and the typical survival probability results.

For the case $p(\tau) = \delta(\tau - \tau_0)$, we get $\overline{S_m} = S_m^* = \exp(m \log q(\tau_0))$, and $\mathcal{T} = m\tau_0$. In the limit $\tau_0 \rightarrow 0$, $m \rightarrow \infty$ with \mathcal{T} kept constant (frequent measurements at close intervals), using Eq. (28) and the fact that $|\psi(0)\rangle$ is normalized to unity, it then follows that $\overline{S_m} = S_m^* = 1 - m\mathcal{O}(\tau_0^2)$. This result implies that to leading order, there is no evolution of the initial state, an illustration of the quantum Zeno effect [4].

For **Scheme 2**, a semi-analytic approach to obtain $|\psi_m^{(a)}\rangle$ along the lines employed for the QRW and detailed in Section 2.2.2, involves the following steps:

- (i) For the initial state $|\psi(0)\rangle = |n_0\rangle$ so that $\psi_{n,n_0}(0) = \delta_{n,n_0}$, we have the discrete Fourier transform $\widehat{\psi}_{q|n_0}(0) = \exp(-i2\pi n_0 q/N)$ for $0 \leq q \leq N-1$.
- (ii) Subsequently, $\widehat{\psi}_{q|n_0}(\tau_1)$, as the outcome of evolution according to (37) for a random time τ_1 sampled according to either the exponential distribution (40) or the power-law distribution (41) and with $\widehat{\psi}_{q|n_0}(0)$ as the initial condition, is obtained as

$$\widehat{\psi}_{q|n_0}(\tau_1) = \widehat{\psi}_{q|n_0}(0) e^{i2\gamma\tau_1 \cos(2\pi q/N)}. \quad (46)$$

- (iii) Inverse discrete Fourier transform of the set $\{\widehat{\psi}_{q|n_0}(\tau_1)\}_{0 \leq q \leq N-1}$ yields the set $\{\psi_{n,n_0}(\tau_1)\}_{0 \leq n \leq N-1}$. The result of a projective measurement at the end of evolution for time τ_1 to obtain the corresponding leftover component of the state is then given by the set $\{\psi_{n,n_0}(\tau_1)\}_{0 \leq n \leq N-1}$ with $\psi_{n_0,n_0}(\tau_1) = 0$.
- (iv) We apply steps 1–3 in turn to the leftover component of the state corresponding to last projection, to finally obtain the survival probability S_m for a given realization $\{\tau_\alpha\}_{1 \leq \alpha \leq m}$ of the dynamics.

Figure 15 shows a very good agreement for both the average and the typical survival probability between the numerical results and those obtained based on the aforementioned semi-analytic approach.

4. Conclusions

In this work, we studied the issue of what happens when a quantum system undergoing unitary evolution in time is subject to repeated projective measurements to the initial state at random times. We considered two distinct dynamical scenarios: **Scheme 1**, in which the evolution after every projective measurement continues with the projected component of the instantaneous state, and **Scheme 2**, in which the evolution continues with the leftover component of the instantaneous state after a measurement has been performed. We focused on a physical quantity of relevance, namely, the survival probability of the initial state after a certain number m of measurements have been performed on the system. Based on results derived for two representative quantum systems defined on a one-dimensional periodic lattice with a finite number of sites N , (i) the quantum random walk evolving in discrete time and (ii) the tight-binding model

evolving in continuous time, we showed that in **Scheme 1**, both the average (averaged with respect to different realizations of the set of random time intervals $\{\tau_\alpha\}_{1 \leq \alpha \leq m}$ between successive measurements) and the typical survival probability (obtained in a typical realization of the set $\{\tau_\alpha\}_{1 \leq \alpha \leq m}$) decay as an exponential in m for large m . One obtains under **Scheme 2** by stark contrast to **Scheme 1** that the behaviour of the survival probability is characterized by two characteristic m values, namely, $m_1^*(N) \sim N$ and $m_2^*(N) \sim N^\delta$ with $\delta > 1$. These scales are such that (i) for m large and satisfying $m < m_1^*(N)$, the decay of the survival probability is as m^{-2} , (ii) for m satisfying $m_1^*(N) \ll m < m_2^*(N)$, the decay is as $m^{-3/2}$, while (iii) for $m \gg m_2^*(N)$, the decay is as an exponential. These results hold independently of the choice of the distribution of times τ_α . We demonstrate this on the basis of our results obtained for a wide range of distributions including exponential and power-law distributions as well as for the case of measurements at regular intervals. It would be interesting to extend our studies to the case of a many-body quantum system where additional dynamical timescales may interplay with the average time between successive measurements to dictate rich static and dynamical behavior.

5. Acknowledgements

The authors acknowledge fruitful discussions with Ashik Iqbal. SG is grateful to Stefano Gherardini and Haggai Landa for insightful preliminary discussions. SG acknowledges support from the Science and Engineering Research Board (SERB), India under SERB-TARE scheme Grant No. TAR/2018/000023, SERB-MATRICES scheme Grant No. MTR/2019/000560, and SERB-CRG scheme Grant No. CRG/2020/000596. Part of this work was carried out using computational facilities of the Advanced Computing Research Centre, University of Bristol, UK - <http://www.bristol.ac.uk/acrc/>. We thank the anonymous referee for making a number of useful suggestions that helped us improve the presentation significantly.

- [1] In this work, we take the Planck's constant to be unity.
- [2] C. Cohen-Tannoudji, B. Diu, and F. Laloë, *Quantum Mechanics, Volume 1: Basic Concepts, Tools, and Applications, 2nd Edition* (Wiley-Interscience, 2006).
- [3] Specifically, the time evolution follows the tight-binding model dynamics discussed later, in Section 3.
- [4] B. Misra and E. C. G. Sudarshan, *The Zeno's paradox in quantum theory*, J. Math. Phys. **18**, 756 (1977).
- [5] S. Gherardini, S. Gupta, F. S. Cataliotti, A. Smerzi, F. Caruso, and S. Ruffo, *Stochastic quantum Zeno by large deviation theory*, New J. Phys. **18**, 013048 (2016).
- [6] Y. Aharonov, L. Davidovich, and N. Zagury, *Quantum random walks*, Phys. Rev. A **48**, 1687 (1993).
- [7] D. H. Dunlap and V. M. Kenkre, *Dynamic localization of a charged particle moving under the influence of an electric field*, Phys. Rev. B **34**, 3625 (1986).
- [8] D. H. Dunlap and V. M. Kenkre, *Dynamic localization of a particle in an electric field viewed in momentum space: Connection with Bloch oscillations*, Phys. Lett. A **127**, 438 (1988).

- [9] M M. Müller, S. Gherardini, and F. Caruso, *Quantum Zeno dynamics through stochastic protocols*, Ann. Phys. **529**, 1600206 (2017).
- [10] S. Gherardini, C. Lovecchio, M. M. Müller, P. Lombardi, F. Caruso, and F. S. Cataliotti, *Ergodicity in randomly perturbed quantum systems*, Quantum Sci. Technol. **2** (1), 015007 (2017).
- [11] S. Gherardini, L. Buffoni, M. M. Müller, F. Caruso, M. Campisi, A. Trombettoni, and S. Ruffo, *Nonequilibrium quantum-heat statistics under stochastic projective measurements*, Phys. Rev. E **98**, 032108 (2018).
- [12] H.-V. Do, C. Lovecchio, I. Mastroserio, N. Fabbri, F. S. Cataliotti, S. Gherardini, M. M. Müller, N. D. Pozza, and F. Caruso, *Experimental proof of quantum Zeno-assisted noise sensing*, New J. Phys. **21**, 113056 (2019).
- [13] S. Dhar, S. Dasgupta, and A. Dhar, *Quantum time of arrival distribution in a simple lattice model*, J. Phys. A: Math. Theor. **48**, 115304 (2015).
- [14] S. Dhar, S. Dasgupta, A. Dhar, and D. Sen, *Detection of a quantum particle on a lattice under repeated projective measurements*, Phys. Rev. A **91**, 062115 (2015).
- [15] H. Friedman, D. A. Kessler, and E. Barkai, *Quantum renewal equation for the first detection time of a quantum walk*, J. Phys. A: Math. Theor. **50**, 04LT01 (2017).
- [16] H. Friedman, D. A. Kessler, and E. Barkai, *Quantum walks: The first detected passage time problem*, Phys. Rev. E **95**, 032141 (2017).
- [17] F. Thiel, E. Barkai, and D. A. Kessler, *First detected arrival of a quantum walker on an infinite line*, Phys. Rev. Lett. **120**, 040502 (2018).
- [18] F. Thiel, I. Mualem, D. A. Kessler, and E. Barkai, *Quantum total detection probability from repeated measurements II. Exploiting symmetry*, arXiv:1909.02114.
- [19] S. Lahiri and A. Dhar, *Return to the origin problem for a particle on a one-dimensional lattice with quasi-Zeno dynamics*, Phys. Rev. A **99**, 012101 (2019).
- [20] D. Meidan, E. Barkai and D. A Kessler, *Running measurement protocol for the quantum first-detection problem*, J. Phys. A: Math. Theor. **52**, 354001 (2019).
- [21] R. Yin, K. Ziegler, F. Thiel, and E. Barkai, *Large fluctuations of the first detected quantum return time*, Phys. Rev. Research **1**, 033086 (2019).
- [22] F. Thiel, I. Mualem, D. Meidan, E. Barkai, and D. A. Kessler, *Dark states of quantum search cause imperfect detection*, Phys. Rev. Research **2**, 043107 (2020).
- [23] F. Thiel, I. Mualem, D. A. Kessler, and E. Barkai, *Uncertainty and symmetry bounds for the quantum total detection probability*, Phys. Rev. Research **2**, 023392 (2020).
- [24] V. Dubey, C. Bernardin, and A. Dhar, *Quantum dynamics under continuous projective measurements: Non-Hermitian description and the continuum-space limit*, Phys. Rev. A **103**, 032221 (2021).
- [25] F. Thiel, I. Mualem, D. Kessler, and E. Barkai, *Uncertainty relation between detection probability and energy fluctuations*, Entropy **23**, 595 (2021).
- [26] Q. Liu, K. Ziegler, D. A. Kessler, and E. Barkai, *Driving quantum systems with repeated conditional measurements*, arXiv:2104.06232.
- [27] D. A. Kessler, E. Barkai, and K. Ziegler, *First-detection time of a quantum state under random probing*, Phys. Rev. A **103**, 022222 (2021).
- [28] R. Ellis, *Entropy, Large Deviations, and Statistical Mechanics* (Springer-Verlag, Berlin, 2006).
- [29] H. Touchette, *The large deviation approach to statistical mechanics*, Phys. Rep. **478**, 1 (2009).
- [30] A. Nayak and A. Vishwanath, *Quantum walk on a line*, arXiv:quant-ph/0010117.
- [31] J. Kempe, *Quantum random walks: an introductory overview*, Contemporary Physics **44**, 307 (2003).
- [32] We use the notation $p(\tau)$ (respectively, p_τ) to denote the distribution for the case when τ is a continuous (respectively, a discrete) variable.

Appendix A. Derivation of Eq. (31) of the main text

In this appendix, we briefly discuss the large deviation (LD) formalism to obtain Eq. (31) of the main text, following Ref. [5]. To proceed, let us specialize to the case of p_τ being a d -dimensional Bernoulli distribution. In other words, we consider the situation in which τ takes on d possible discrete values $\tau^{(1)}, \tau^{(2)}, \dots, \tau^{(d)}$, with corresponding probabilities $p^{(1)}, p^{(2)}, \dots, p^{(d)}$ satisfying $\sum_{\alpha=1}^d p^{(\alpha)} = 1$. To invoke the LD formalism for the survival probability, consider the quantity

$$\mathcal{L}(\{\tau_\alpha\}_{1 \leq \alpha \leq m}) \equiv \log(S_m(\{\tau_\alpha\}_{1 \leq \alpha \leq m})) = \sum_{\alpha=1}^d n_\alpha \log q(\tau^{(\alpha)}), \quad (\text{A.1})$$

where we have denoted by n_α the number of times the value $\tau^{(\alpha)}$ occurs in the sequence $\{\tau_\alpha\}_{1 \leq \alpha \leq m}$. The quantity \mathcal{L} is a sum of i.i.d. random variables, and its probability distribution is evidently given by (see Ref. [5])

$$\mathcal{P}(\mathcal{L}) = \frac{m!}{n'_1! n'_2! \dots n'_d!} \prod_{\alpha=1}^d (p^{(\alpha)})^{n'_\alpha}, \quad (\text{A.2})$$

where the quantities n'_α satisfy the two constraints $\sum_{\alpha=1}^d n'_\alpha = m$ and $\sum_{\alpha=1}^d n'_\alpha \log q(\tau^{(\alpha)}) = \mathcal{L}$, implying that one has $m \log q(\tau^{(d)}) - \mathcal{L} = \sum_{\alpha=1}^{d-1} n'_\alpha \lambda(\tau^{(\alpha)})$, with $\lambda(\tau^{(\alpha)}) \equiv \log q(\tau^{(d)}) - \log q(\tau^{(\alpha)})$. The solution is [5]

$$n'_\alpha = \frac{m \log q(\tau^{(d)}) - \mathcal{L}}{(d-1) \lambda(\tau^{(\alpha)})}; \quad \alpha = 1, 2, \dots, d-1, \quad (\text{A.3})$$

and $n'_d = m - \sum_{\alpha=1}^{d-1} n'_\alpha$. Using this solution in Eq. (A.2), it may be shown that in the limit $m \rightarrow \infty$, the distribution $\mathcal{P}(\mathcal{L})$ has the following LD form [5]

$$\mathcal{P}(\mathcal{L}) \rightarrow \mathcal{P}(\mathcal{L}/m) \approx \exp(-mI(\mathcal{L}/m)), \quad (\text{A.4})$$

with

$$I(x) \equiv \sum_{\alpha=1}^d f(\tau^{(\alpha)}) \log \left(\frac{f(\tau^{(\alpha)})}{p^{(\alpha)}} \right), \quad (\text{A.5})$$

$$f(\tau^{(\alpha)}) \equiv \frac{\log q(\tau^{(d)}) - x}{(d-1)\lambda(\tau^{(\alpha)})}; \quad \alpha = 1, \dots, (d-1), \quad (\text{A.6})$$

$$f(\tau^{(d)}) \equiv 1 - \sum_{\alpha=1}^{d-1} f(\tau^{(\alpha)}). \quad (\text{A.7})$$

From Eq. (A.4), it follows that the minimum of the function $I(\mathcal{L}/m)$ corresponds to the most probable value \mathcal{L}^* of \mathcal{L} as $m \rightarrow \infty$. From Eq. (A.5), the

condition $\partial I(\mathcal{L}/m)/\partial \log q(\tau^{(\alpha)})|_{\mathcal{L}=\mathcal{L}^*} = 0$ gives, on performing a series of algebraic manipulations, that [5]

$$\mathcal{L}^* = m \sum_{\alpha=1}^d p^{(\alpha)} \log q(\tau^{(\alpha)}). \quad (\text{A.8})$$

Using Eqs. (A.1) and (A.4), one may obtain an LD form for the distribution of the survival probability S_m as [5]

$$\mathcal{P}(S_m) \approx \exp(-m J(S_m)), \quad (\text{A.9})$$

with $J(S_m) \equiv \min_{\mathcal{L}: \mathcal{L}=\log S_m} I(\mathcal{L}/m)$. The value S_m^* that minimizes the function $J(S_m)$ is the most probable value of the survival probability in the limit $m \rightarrow \infty$; one gets [5]

$$S_m^* = \exp\left(m \sum_{\alpha=1}^d p^{(\alpha)} \log q(\tau^{(\alpha)})\right), \quad (\text{A.10})$$

which rewritten suitably yields Eq. (31) of the main text.